Check for updates

JGR Oceans

RESEARCH ARTICLE
10.1029/2022JC019121

Key Points:

- In the mid-latitudes, the seasonal cycle (64.7%) and climate variability (9.6%) combine to explain 74.3% of satellite chlorophyll variance
- In the tropics, the seasonal cycle (30.9%) and climate variability (26.3%) combine to explain 57.2% of satellite chlorophyll variance
- Delayed climate effects (a season ahead) provide a source of interannual chlorophyll predictability in the tropics (39.7%)

Supporting Information:

Supporting Information may be found in the online version of this article.

Correspondence to:

H.-G. Lim,
hyl021@ucsd.edu

Citation:

Lim, H.-G., Dunne, J. P., Stock, C. A., & Kwon, M. (2022). Attribution and predictability of climate-driven variability in global ocean color. *Journal of Geophysical Research: Oceans*, *127*, e2022JC019121. https://doi.org/10.1029/2022JC019121

Received 23 JUL 2022
Accepted 10 OCT 2022

Author Contributions:

Conceptualization: Hyung-Gyu Lim, John P. Dunne, Charles A. Stock
Formal analysis: Hyung-Gyu Lim
Funding acquisition: John P. Dunne
Investigation: Hyung-Gyu Lim
Methodology: Hyung-Gyu Lim, John P. Dunne, Charles A. Stock, Minho Kwon
Resources: John P. Dunne
Software: Hyung-Gyu Lim
Supervision: John P. Dunne, Charles A. Stock

© 2022 The Authors. This article has been contributed to by U.S. Government employees and their work is in the public domain in the USA.
This is an open access article under the terms of the Creative Commons Attribution-NonCommercial License, which permits use, distribution and reproduction in any medium, provided the original work is properly cited and is not used for commercial purposes.

Attribution and Predictability of Climate-Driven Variability in Global Ocean Color

Hyung-Gyu Lim[1,2], John P. Dunne[3], Charles A. Stock[3], and Minho Kwon[4]

[1]Princeton University/Atmospheric and Oceanic Sciences Program, Princeton, NJ, USA, [2]Scripps Institution of Oceanography, University of California San Diego, San Diego, CA, USA, [3]NOAA/OAR/Geophysical Fluid Dynamics Laboratory, Princeton, NJ, USA, [4]Korea Institute Ocean Science and Technology, Busan, South Korea

Abstract For over two decades, satellite ocean color missions have revealed spatio-temporal variations in marine chlorophyll. Seasonal cycles and interannual changes of the physical environment drive the nutrient and chlorophyll variations. In order to identify contributions of seasonal and interannual components on chlorophyll, the present study investigates total chlorophyll variance (TCV) of a 24 year records (September 1997 to December 2021) across satellite generations. First-order contributions of the seasonal cycle in the mid-latitude (25°–35°) oceans in the Northern and Southern Hemispheres explain 59.5% and 69.9% of TCV, respectively. In contrast, the contribution of seasonal cycle only explain 30.9% in the tropical oceans (20°N–20°S). Both seasonal cycle- and climate-driven variability (26.3%) explain 57.2% on TCV in the tropical oceans. A multiple linear regression model was forced by instantaneous and delayed effects of oceanic memory of eight climate indices based on sea surface temperature anomalies to reconstruct chlorophyll anomalies. Delayed climate effects generally boost the anomaly correlation coefficients (ACC) between the observed and reconstructed chlorophyll timeseries (ACC skills: 0.64 to 0.72 in the Indian Ocean, 0.74 to 0.82 in off-equatorial Northern Pacific, and 0.58 to 0.71 in the off-equatorial Southern Pacific). Such delayed climate effects provide a source of predicted chlorophyll ACC (ACC_predic) skills one season ahead in some ocean regions (ACC_predic skill: 0.63 in the overall tropical ocean, 0.67 in the tropical Pacific, and 0.60 in the Indian Ocean). The attribution of chlorophyll variability indicates promising avenues for improving marine ecosystem predictions with Earth system models by incorporating delayed climate effects.

Plain Language Summary Surface ocean color detected by satellites can be used to estimate the photosynthetic pigment chlorophyll used by phytoplankton at the base of ocean food chains. Satellites show that chlorophyll varies in space and time. In this study, we identify chlorophyll time variation as it is influenced by two components: (a) the seasonal cycle, (b) interannual variations. We find that the seasonal cycle dominates chlorophyll variance in the mid latitudes. However, the seasonal cycle explains less than a third of tropical chlorophyll variance. The addition of interannual climate-driven changes explains over half of tropical chlorophyll variance. We used a statistical model of chlorophyll based on eight different indices of year-to-year climate fluctuations in sea surface temperature to further understand the influence of current and past conditions on its variance. Delayed effects of sea surface temperature from prior seasons improve model estimates of chlorophyll in the equatorial Pacific and Indian Oceans. Thus, ocean "memory" of sea surface temperature variability can be a source of substantial skill in tropical chlorophyll predictability for future seasons.

1. Introduction

Since September 1997, high quality records in satellite ocean color have continuously revealed spatio-temporal variations in chlorophyll concentration, a proxy for phytoplankton biomass, at a near-global scale. The chlorophyll concentration data set has been a focal point in estimating myriad properties, including but not limited to global marine primary production (Carr et al., 2006; Falkowski, 1994), phytoplankton bloom dynamics (Ardyna et al., 2014; Arrigo, 2003; Henson et al., 2009; Yamaguchi et al., 2022), light attenuation coefficients in ocean layers (Manizza et al., 2005; Morel, 1988), carbon export (Dunne et al., 2007; Henson et al., 2012), fish species distribution (Cheung et al., 2010; Hazen et al., 2018) and fisheries catch (Chassot et al., 2010; Friedland et al., 2012; Park et al., 2019). The variation of chlorophyll concentration has also played a crucial role in validating predictive physical-biogeochemical models and is being assimilated into biogeochemical state estimates (Dutkiewicz et al., 2020; Fennel et al., 2019).

21699291, 2022, 10, Downloaded from https://agupubs.onlinelibrary.wiley.com/doi/10.1029/2022JC019121, Wiley Online Library on [22/10/2022]. See the Terms and Conditions (https://onlinelibrary.wiley.com/terms-and-conditions) on Wiley Online Library for rules of use; OA articles are governed by the applicable Creative Commons License

Validation: Hyung-Gyu Lim, Minho Kwon
Visualization: Hyung-Gyu Lim
Writing – original draft: Hyung-Gyu Lim
Writing – review & editing: Hyung-Gyu Lim, John P. Dunne, Charles A. Stock, Minho Kwon

The variation in chlorophyll concentration is closely associated with the oceanic physical environment. The highly productive regions are located in areas of strong upwelling, boundary currents, and/or mid-to high-latitudes systems (Banse, 1992; Everett et al., 2014; Falkowski & Woodhead, 2013; Kämpf & Chapman, 2016; Murray et al., 1992). In contrast, the least productive regions, so-called oligotrophic waters, are located in the subtropical gyres (Laws et al., 1987; Polovina et al., 2008; Sarmiento et al., 2004; Signorini et al., 2015). These regions have unfavorable physical conditions for the supply of nutrients due to stabilized ocean layers, negative windstress curl, and downwelling (Talley et al., 2011). Seasonal changes in light, stratification and nutrient supply (Dave et al., 2015; Signorini et al., 2015) also drive the migration of chlorophyll fronts at the boundaries between mesotrophic and oligotrophic waters (Polovina et al., 2017; Vantrepotte & Mélin, 2009; Yoder & Kennelly, 2003) and the seasonal dependency of chlorophyll extremes driven by marine heatwaves (Noh et al., 2022).

Despite the prominence of seasonal drivers of chlorophyll variability, the year-to-year (i.e., interannual) changes of the physical environment in some regions may drive a more substantial chlorophyll variation. In the tropical Pacific, the El Niño–Southern Oscillation (ENSO) (McPhaden et al., 2006), the most prominent mode of climate variability, strongly alters the equatorial Pacific thermocline, nutrient upwelling, and chlorophyll (climatology: 0.2 ug/L) fluctuations from lowest record 0.05 μg/L (four-fold smaller than climatology) to about 1 μg/L (five-fold larger than climatology) (Behrenfeld et al., 2001; Chavez et al., 1999; Murtugudde et al., 1999). ENSO is a major contributor in global chlorophyll fluctuation associated with changes in physical and biological environments (Chavez et al., 2011). The evolution of ENSO modulates the tropical Pacific chlorophyll responses from a basin-wide pattern in boreal winter to 6 month delayed tri-polar pattern in boreal summer, positive anomalies along the equator and negative anomalies in off-equator in El Niño events (Park et al., 2011). In the equatorial Pacific, the ENSO-chlorophyll evolution in boreal summer is associated with post-El Niño iron rebound (Lim et al., 2022).

In addition to ENSO, the Pacific Decadal Oscillation (PDO) (Mantua et al., 1997) and the North Pacific Gyre Oscillation (NPGO) (Di Lorenzo et al., 2008) are leading modes of the extra-tropical Pacific climate that interact with the tropical Pacific via atmospheric (Alexander et al., 2002; Trenberth & Hurrell, 1995; Vimont, 2005; Yeh et al., 2018) and oceanic (Amaya, 2019; Di Lorenzo et al., 2010; Joh & Di Lorenzo, 2019; Vimont et al., 2009; Walker & Bliss, 1932) teleconnections. Linear model reconstruction with combined large-scale Pacific climate variabilities (ENSO, PDO, and NPGO) explains the variance of chlorophyll anomalies in the Pacific ocean basin, locally upto 70% estimated by 13-year satellite ocean color (Di Lorenzo et al., 2013).

Investigation of climate variability modes has also revealed delayed relationships between the tropical ocean basins (Cai et al., 2019; Ham, Kug, Park, et al., 2013; Jiang et al., 2021; Kug & Kang, 2006; Park, Kug, et al., 2018) with implications for predictability and of potential practical utility to prediction systems (Izumo et al., 2010; Jeong et al., 2021; Luo et al., 2017). The climate variability in the Indian Ocean does not only alter the mixed layer depth, nutrients, and chlorophyll anomalies in the internal Indian Ocean (Murtugudde et al., 1999; Park & Kug, 2014), but also generates the delayed remote effect in the equatorial Pacific chlorophyll rebound (Tian et al., 2021). In addition, the Atlantic Niño has not only characterized positive sea surface temperature and sea surface height anomalies in the internal Atlantic Ocean (Vallès-Casanova et al., 2020; Zebiak, 1993), but also drives the delayed remote impact on ENSO variability in the tropical Pacific (Ham, Kug, & Park, 2013).

The attribution study of the chlorophyll variance from 10-years of satellite ocean color (Vantrepotte & Mélin, 2009) is in need of an update for the full 24-years record of global ocean color. In addition, the report for chlorophyll variance contribution using linear model reconstruction for 13-year chlorophyll anomalies based on instantaneous ENSO, PDO, and NPGO indices (Di Lorenzo et al., 2013) can be improved by considering delayed effects of climate indices. In this study, we revisit global ocean color estimates of chlorophyll for 24-years from September 1997 to December 2021 and investigate the contribution from the seasonal cycle and interannual climate components on TCV building upon previous studies. We first quantitatively estimate the importance of the seasonal cycle on TCV and subsequently estimate the role of climate variability, focusing on instantaneous and delayed responses to eight climate modes that are indicative of potentially predictable chlorophyll responses. Section 2 describes the data set and assessment metrics in seasonal and interannual components of global TCV. Sections 3.1–3.3 shows results of global TCV and decomposition approaches from seasonal and interannual components driven by climate variability. Section 3.4 uses the delayed components of climate states from prior seasons to assess the statistical predictability of chlorophyll. Section 4 summarizes the climate drivers of chlorophyll variance, their implications for predictability, and related results herein to past findings on this topic.

21699291, 2022, 10, Downloaded from https://agupubs.onlinelibrary.wiley.com/doi/10.1029/2022JC019121, Wiley Online Library on [22/10/2022]. See the Terms and Conditions (https://onlinelibrary.wiley.com/terms-and-conditions) on Wiley Online Library for rules of use; OA articles are governed by the applicable Creative Commons License

Table 1
List of Climate Indices Using Sea Surface Temperature Anomalies (SSTa) Implemented in the Multiple Linear Regression (MLR) Model for Reconstructions of Chlorophyll Anomalies (rCHLa)

Climate variability	Index	SSTa index domain	Reference
Eastern Pacific (Cold Tongue) ENSO	NINO3	(5°N–5°S, 150°W–90°W)	Trenberth (1997); Kug et al. (2009); Yeh et al. (2009)
Central Pacific (Warmpool) ENSO	NINO4	(5°N–5°S, 160°E–150°W)	
Pacific decadal oscillation	PDO	EOF 1st PC (120°E–60°W, 20°N–60°N)	Mantua et al. (1997)
North Pacific gyre oscillation (Victoria Mode)	NPGO	EOF 2nd PC (120°E–60°W, 20°N–60°N)	Bond et al. (2003); Di Lorenzo et al. (2008)
Atlantic Niño	ATL3	(20°W–0°, 3°S–3°N)	Zebiak (1993); Vallès-Casanova et al. (2020)
Atlantic meridional mode	AMM	(5°–15°N, 50°–20°W) minus (5°–15°S, 20°W–10°E)	Xie and Carton (2004); Doi et al. (2010)
Indian Ocean dipole mode	DMI	(50°E–70°E, 10°S–10°N) minus (90°E–110°E,10°S–0°)	Saji et al. (1999)
Indian Ocean basin mode	IOBM	(20°S–20°N, 40°–105°E)	Klein et al. (1999); Hong et al. (2010)

Note. SSTa are obtained from SST by subtracting the monthly climatology of SST from 1951 to 2019. All climate indices were used from September 1997 to December 2021 to match global ocean color datasets. Pacific Decadal Oscillation (PDO) and North Pacific Gyre Oscillation (NPGO)-like indices are generated by an Empirical Orthogonal Function (EOF) of North Pacific SSTa from 1951 to 2021 to capture long-term variabilities and only the first (PDO) and second (NPGO) Principle Component (PC) timeseries of the EOF from September 1997 to December 2021 were used in the MLR model.

Section 4 also discusses potential drivers of unexplained chlorophyll variance and their potential incorporation into predictive models.

2. Methods

2.1. Data Set

For the analysis, we used global ocean color satellite-derived chlorophyll concentration products from September 1997 to December 2021. For the main result, we used Garver, Siegel, Maritorena (GSM) model product in GlobColour (GlobColour-GSM) for Case 1 water (Maritorena et al., 2010). The bio-optical model procedure of GSM model and its general features are described in Maritorena et al. (2002) and Maritorena and Siegel (2005). This product uses normalized reflectances at the original sensor wavelengths of satellite generations, without intercalibration. GlobColour-GSM product (100 km horizontal resolution) was obtained from the GlobColour version 2021.1 (https://hermes.acri.fr). To use the full timeseries for monthly satellite coverage, our analysis was restricted to the open ocean, latitudes 50°N-50°S, excluding the seasonal sea ice cover areas.

In the supplemental results, we compare two different satellite product: (a) GlobColour satellite product merged by the simple average method model (GlobColour-AVM), obtained from https://hermes.acri.fr; (b) European Space Agency Ocean Colour Climate Change Initiative project version 5.0 (ESA-OC-CCI-v5.0), a blended version of combination of OCI, OCI2, OC2, and OCx algorithms (Sathyendranath et al., 2021). We obtained 4 km horizontal resolution of ESA-OC-CCI-v5.0, obtained from https://climate.esa.int/en/projects/ocean-colour/ and ESA-OC-CCI-v5.0 data set was regridded by bilinear interpolation of climate data operators (remapbil) into 100 km. GlobColour-AVM and ESA-OC-CCI-v5.0 were used to benchmark the robustness of main result of GlobColour-GSM.

For the calculation of major climate indices (Table 1), sea surface temperature (SST) data was obtained from the NOAA Extended Reconstructed SST version 5 (ERSST v5) (Huang et al., 2017).

Linear trends based on least-squares fitting over time in all datasets show global chlorophyll declines in tropical and midlatitude oceans (Figure S1 in Supporting Information S1), consistent with Boyce et al. (2014) but increasing trends of chlorophyll occur in the Humbolt current near the westcoast of South America and in polar regions. In this study, we remove these linear trends over time from all data sets as attributions are challenging to interpret due to the inconsistency of patterns and magnitudes of linear trends between chlorophyll products (Figure S1 in Supporting Information S1), which have sources of linear trend uncertainty in ocean optics of phytoplankton communities (Dutkiewicz et al., 2019). This choice also helps avoid the misinterpretation of multidecadal climate variation and climate change effects due to relatively short timeseries (~24 years) relative to these signals. We

21699291, 2022, 10, Downloaded from https://agupubs.onlinelibrary.wiley.com/doi/10.1029/2022JC019121, Wiley Online Library on [22/10/2022]. See the Terms and Conditions (https://onlinelibrary.wiley.com/terms-and-conditions) on Wiley Online Library for rules of use; OA articles are governed by the applicable Creative Commons License

also note that these trends contributed only a small fraction (2%–6% difference TCVs between with and without linear trends) to global TCV over the analysis period (not shown).

2.2. Chlorophyll Variance Analysis

Using GlobColour-GSM, GlobColour-AVM, and ESA-OC-CCI-v5.0, we defined TCV at a given grid cell of chlorophyll timeseries (CHL_t),

$$\mathrm{TCV} = \frac{1}{n}\sum_{t=1}^{n}(\mathrm{CHL}_t - \mu)^2 \tag{1}$$

where n is equal to degree of freedom of chlorophyll datasets (288 month for 24 years from September 1997 to August 2021), μ is equal to the mean annual chlorophyll over the 24 year analysis period after detrending CHL_t,

$$\mu = \frac{1}{n}\sum_{t=1}^{n}\mathrm{CHL}_t \tag{2}$$

TCV includes both seasonal and interannual components in chlorophyll. We note that the seasonal cycle of chlorophyll and interannual chlorophyll anomaly are independent. Correlation coefficient between seasonal and interannual chlorophyll timeseries is almost zero (not shown). Thus, TCV can be separated by seasonal and interannual components.

The first order component in TCV is the seasonal variation (Vantrepotte & Mélin, 2009; Yoder & Kennelly, 2003). We defined the variance in chlorophyll based on the seasonal cycle (SCV),

$$\mathrm{SCV} = \frac{1}{n}\sum_{t=1}^{n}(\mathrm{CHL_SC}_t - \mu)^2 \tag{3}$$

where $\mathrm{CHL_SC}_t$ is chlorophyll climatology of all calendar month from September 1997 to August 2021 and repeating monthly values of calculated chlorophyll climatology with time. The observed patterns of TCV and SCV are shown in Section 3.1.

The residual variance after excluding SCV is referred to as the anomalous chlorophyll variance (ACV). That is,

$$\mathrm{ACV} = \mathrm{TCV} - \mathrm{SCV} = \frac{1}{n}\sum_{t=1}^{n}(\mathrm{CHLa}_t)^2 \tag{4}$$

where CHLa_t is equal to chlorophyll anomalies. CHLa_t is calculated by removing $\mathrm{CHL_SC}_t$ from the detrended CHL_t.

2.3. Reconstruction of Chlorophyll Variance

Identifying CHLa_t allows us to associate the variance in CHLa_t with dominant climate modes using their partial linear regression coefficients (β) in a multiple linear regression (MLR) model for CHLa_t, as shown in Equation 5. First, we define climate indices simply using only SST anomalies obtained from ERSSTv5, as shown in Table 1. All climate indices were normalized by their standard deviation. Then, β is forced by each instantaneous and delayed climate mode against satellite chlorophyll time series observed at each grid cell, with the relationships quantifying "delayed effects" indicative of predictability in the system. Using β and climate indices, we calculated reconstructed chlorophyll anomaly timeseries ($\mathrm{rCHL}_t{}'$):

$$\begin{aligned}\mathrm{rCHLa}_t = \sum_{\tau=0}^{4}(&\beta_{1,t-\tau}\cdot\mathrm{NINO3}_{t-\tau} + \beta_{2,t-\tau}\cdot\mathrm{NINO4}_{t-\tau} + \beta_{3,t-\tau}\cdot\mathrm{PDO}_{t-\tau}\\ &+ \beta_{4,t-\tau}\cdot\mathrm{NPGO}_{t-\tau} + \beta_{5,t-\tau}\cdot\mathrm{ATL3}_{t-\tau} + \beta_{6,t-\tau}\cdot\mathrm{AMM}_{t-\tau}\\ &+ \beta_{7,t-\tau}\cdot I\mathrm{OBM}_{t-\tau} + \beta_{8,t-\tau}\cdot\mathrm{DMI}_{t-\tau})\end{aligned} \tag{5}$$

where τ is the timescale of instantaneous climate indices ($\tau = 0$) and lagged seasons of climate indices to consider delayed effects ($\tau = 1 - 4$). We tested that considering monthly averaged SSTa climate indices as predictors led the MLR model to be overfitted (not shown). In the present study, we use seasonally averaged SSTa climate

21699291, 2022, 10, Downloaded from https://agupubs.onlinelibrary.wiley.com/doi/10.1029/2022JC019121, Wiley Online Library on [22/10/2022]. See the Terms and Conditions (https://onlinelibrary.wiley.com/terms-and-conditions) on Wiley Online Library for rules of use; OA articles are governed by the applicable Creative Commons License

indices as predictors on MLR model. In this case, $\tau = 1$ means 1–3 lag month average, $\tau = 2$ means 4–6 lag month average, $\tau = 3$ means 7–9 lag month average, $\tau = 4$ means 10–12 lag month average.

We performed the MLR model based on "leave-one-out cross-validation" (hereafter cross-validation). The cross-validation is a broadly applied metric of the statistical models to assess the skills with avoiding the overfitted results (Jeong et al., 2021). For this validation method, a time step (1 month) of observation is omitted from CHLa data sets and climate indices, and rest of time steps (291 month) from CHLa and climate indices are resampled. This resampled data is used to calculate MLR coefficients and reconstructions for an omitted timestep out of resamples. Thus, rCHLa timeseries are generated by the MLR model during multiple times (total 292 times; from September 1997 to December 2021) for every CHLa timeseries by resampled CHLa and climate indices. β is not sensitive to omitted time during cross-validation. The correlation skills between CHLa and rCHLa are shown in Section 3.3.

Using rCHLa_t reconstructed ACV related to major climate modes (rACV) is,

$$\mathrm{rACV} = \frac{1}{n}\sum_{t=1}^{n}(\mathrm{rCHLa}_t)^2 \tag{6}$$

and reconstructed TCV (rTCV) is,

$$\mathrm{rTCV} = \frac{1}{n}\sum_{t=1}^{n}(\mathrm{rCHLa}_t + \mathrm{CHL_SC}_t - \mu)^2 \tag{7}$$

assuming the changes of $\mathrm{CHL_SC}_t$ are negligible in rTCV. All results of rCHLa, rACV, and rTCV shown in the Sections 3.2–3.4 are cross-validated estimate.

2.4. Predicting Chlorophyll Anomaly

The analysis above quantifies the contributions of the seasonal cycle and various elements of climate variability to the overall chlorophyll signal. To explore chlorophyll predictability, we repeat the process of MLR model (Equation 5 in Section 2.3) but predicted rCHLa calculated from delayed climate effects only (rCHLa_predic), summarized in Table S1 in Supporting Information S1. In this case, the instantaneous ($\tau = 0$) climate variability is not considered. The calculation of MLR coefficients between delayed climate indices and CHLa on the target timeseries are cross-validated estimate. To resolve monthly lead time and reduce the number of degrees of freedom, we generate the MLR model based on 3-monthly averaged timeseries from $\tau = 1$ to $\tau = 4$. This predictability approach is similar to the above rCHLa calculations excepting for $\tau = 0$. To see the predictability with increased lead time of delayed effects of climate indices, τ are removed step-wise a month (see Table S1 in Supporting Information S1).

2.5. Anomaly Correlation Coefficient (ACC) Skill Assessment Metric

We calculated ACC skill for assessing the attribution of climate indices on CHLa and its predictability. The ACC calculation is based on the Pearson correlation coefficient to represent normalized covariance coefficient of rCHLa and rCHLa_predic against observed CHLa.

To attribute climate indices on CHLa, we calculate ACC between CHLa and rCHLa,

$$\mathrm{ACC} = \frac{\sum_{t=1}^{n}\mathrm{CHLa}_t \cdot \mathrm{rCHLa}_t}{\sqrt{\sum_{t=1}^{n}\mathrm{CHLa}_t^{\,2}}\cdot\sqrt{\sum_{t=1}^{n}\mathrm{rCHLa}_t^{\,2}}} \tag{8}$$

To assess the predictability, we calculate predicted ACC (ACC_predic) between CHLa and rCHLa_predic,

$$\mathrm{ACC_predic} = \frac{\sum_{t=1}^{n}\mathrm{CHLa}_t \cdot \mathrm{rCHLa_predic}_t}{\sqrt{\sum_{t=1}^{n}\mathrm{CHLa}_t^{\,2}}\cdot\sqrt{\sum_{t=1}^{n}\mathrm{rCHLa_predic}_t^{\,2}}} \tag{9}$$

21699291, 2022, 10, Downloaded from https://agupubs.onlinelibrary.wiley.com/doi/10.1029/2022JC019121, Wiley Online Library on [22/10/2022]. See the Terms and Conditions (https://onlinelibrary.wiley.com/terms-and-conditions) on Wiley Online Library for rules of use; OA articles are governed by the applicable Creative Commons License

3. Results

Results are based on GlobColour-GSM (Figures 1–5). Supporting results are also provided based on GlobColour-AVM and ESA-OC-CCI-v5.0 in Supporting Information S1 (Figures S1–S7) to demonstrate consistency with the GlobColour-GSM results.

3.1. Impact of Seasonal Chlorophyll Variation on TCV

The spatial distribution in TCV (Equation 1) in GlobColour-GSM exhibits relatively high values in the tropical oceans, coastal, and subpolar oceans and relatively low values in subtropical oceans (Figure 1a). Overall, the spatial pattern of TCV in open oceans represents high-low-high patterns, characterized by prominent lows in the subtropical gyres bounded by equatorward and poleward highs. The skyblue line in Figure 1a denotes the edge of oligotrophic waters defined as below 0.07 mg/m^3 of mean annual chlorophyll (Polovina et al., 2008) suggesting that the high-low-high TCV transition is well matched with the transition zone between mesotrophic and oligotrophic waters.

The spatial distribution in SCV (Equation 3) in GlobColour-GSM shows that the absolute contribution of the seasonal cycle is strongest in highly productive coastal regions and high latitude oceans (Figure 1b). SCV exhibits relatively high values in subpolar regions compared to tropical and subtropical oceans. The seasonal variation of dynamic ocean features with physical and biological interaction near the western boundary currents and poleward edges of subtropical gyres likely contribute to high SCV in these regions (Polovina et al., 2017; Signorini et al., 2015).

The percentage contribution of TCV explained by SCV indicates that, generally, the seasonal cycle dominates zonal bands of chlorophyll variance in the midlatitude at the front between subtropical and subpolar gyres in the Southern Indian Ocean and both hemispheres in the Pacific and Atlantic Oceans (Figure 1c), consistent with patterns described in previous assessments using shorter satellite records (Vantrepotte & Mélin, 2009; Yoder & Kennelly, 2003). The maxima in the percentage contribution often do not coincide with the absolute SCV maxima (Figures 1b and 1c). The contribution of seasonal components is 41.8% averaged in 50°N–50°S, maximized in poleward edges of subtropical gyres in mid-latitudes which are 59.5%, zonally averaged in 25°N–35°N, and 69.9%, zonally averaged in 35°S–25°S. In contrast, chlorophyll variance in the tropical ocean basins explained by seasonal components is much less, explaining only 30.9% of TCV, zonally averaged in 20°N–20°S, and implying that other components drive TCV in these regions. GlobColour-AVM and ESA-OC-CCI-v5.0 (Figure S2 in Supporting Information S1) also represent the high contribution of SCV on TCV with high-low-high patterns, which are consistent with the patterns of the Glob-Colour-GSM result (Figure 1c).

3.2. Interannual Variation Components of TCV Associated With Climate-Driven Variability

The global distribution of ACV (Equation 4) in GlobColour-GSM demonstrates that while ACV is minimal in oligotrophic waters, highly productive regions in coastal areas and high latitude oceans generally have high ACV values (Figure 2a). ACV also exhibits a distinctive horseshoe pattern of high values in the tropical Pacific and high values in the equatorial Indian and Atlantic Oceans. Since long-term satellite-derived ocean color has informed historical seasonal and interannual chlorophyll estimates, many of these prominent regional patterns have been described previously (Chavez et al., 1999, 2011; Di Lorenzo et al., 2013; Gorgues et al., 2010; Grodsky et al., 2008; Kang et al., 2017; Lee et al., 2014; Messié & Chavez, 2012; Murtugudde et al., 1999; Park et al., 2011; Park & Kug, 2013; Tian et al., 2021; Zhang et al., 2018), indicating that climate variability may provide mechanisms for ACV attribution (i.e., rACV).

To quantify the role of climate-driven variability in ACV, we applied the MLR approach by fitting climate effects on CHLa to generate rCHLa (Equation 5) and rACV ($\tau = 0 - 4$ in Equation 6). Note that rACV shown in Figure 2b considers not only instantaneous ($\tau = 0$) effects but also delayed effects ($\tau = 1 - 4$) of climate variability due to their memory effects from prior seasons to CHLa next seasons. Attribution of delayed effects of climate variability is further described in Section 3.3.

The general features of rACV (Figure 2b) exhibit patterns similar to ACV (Figure 2a): High explainable chlorophyll variability is apparent in the equatorial ocean and low explainable chlorophyll variability is apparent

21699291, 2022, 10, Downloaded from https://agupubs.onlinelibrary.wiley.com/doi/10.1029/2022JC019121, Wiley Online Library on [22/10/2022]. See the Terms and Conditions (https://onlinelibrary.wiley.com/terms-and-conditions) on Wiley Online Library for rules of use; OA articles are governed by the applicable Creative Commons License

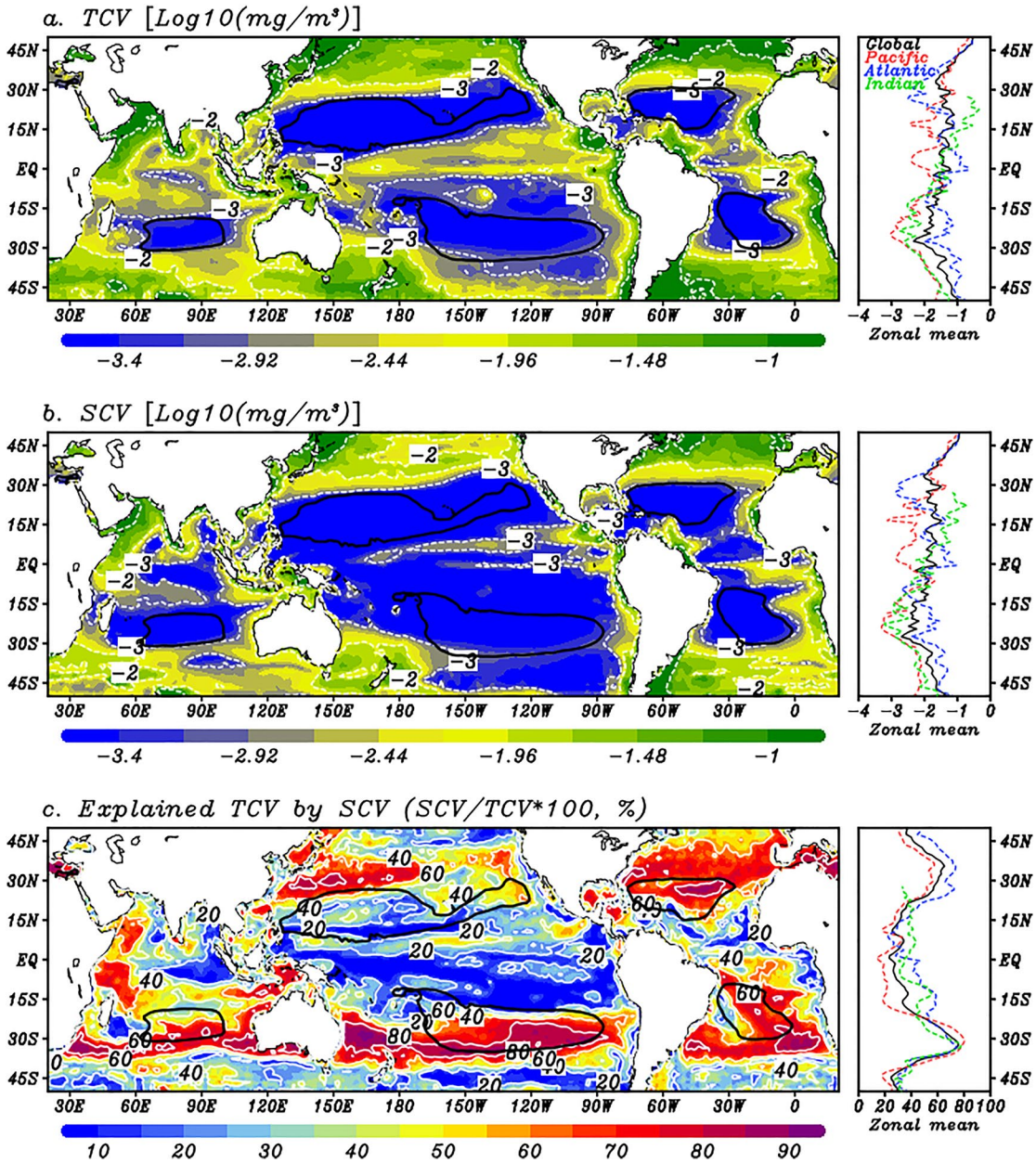

Figure 1. Seasonal cycle controls first order total chlorophyll variance (TCV) in the mid latitude. (a) Log_{10}-transformed TCV from September 1997 to August 2021 (Equation 1), (b) Log_{10}-transformed seasonal cycle (SCV) from September 1997 to August 2021 (Equation 3). TCV and SCV are calculated in original scale of chlorophyll (mg/m^3) and then transformed to log_{10} to represent in global as shown in figures. (c) Explained TCV by seasonal cycle (SCV/TCV*100), which is calculated based on original scale of chlorophyll (mg/m^3). Black contour line denotes the edge of oligotrophic waters defined as below 0.07 mg/m^3 of mean annual chlorophyll.

in oligotrophic waters. As we quantify below, much of the unresolved TCV in tropical oceans based on SCV (Figure 1c) can be explained by the physical and biological responses to interannual climate variation.

The performance of the MLR approach can be evaluated with the spatial pattern of explained TCV based on rTCV (Equation 7) (Figure 2c). Comparing Figures 1c and 2c, we can see that much of the observed TCV pattern averaged in 50°N–50°S can be explained by climate-driven effects reflected in rTCV increased from 41.8% in seasonal component to 60.9% (+19.1%) after including both seasonal and climate variability components. Especially, TCV in the tropical ocean averaged in 20°N–20°S increased from 30.9% in seasonal component to 57.2% (+26.3%) after adding climate-driven variability to seasonal patterns. Even considering the dominant

21699291, 2022, 10, Downloaded from https://agupubs.onlinelibrary.wiley.com/doi/10.1029/2022JC019121, Wiley Online Library on [22/10/2022]. See the Terms and Conditions (https://onlinelibrary.wiley.com/terms-and-conditions) on Wiley Online Library for rules of use; OA articles are governed by the applicable Creative Commons License

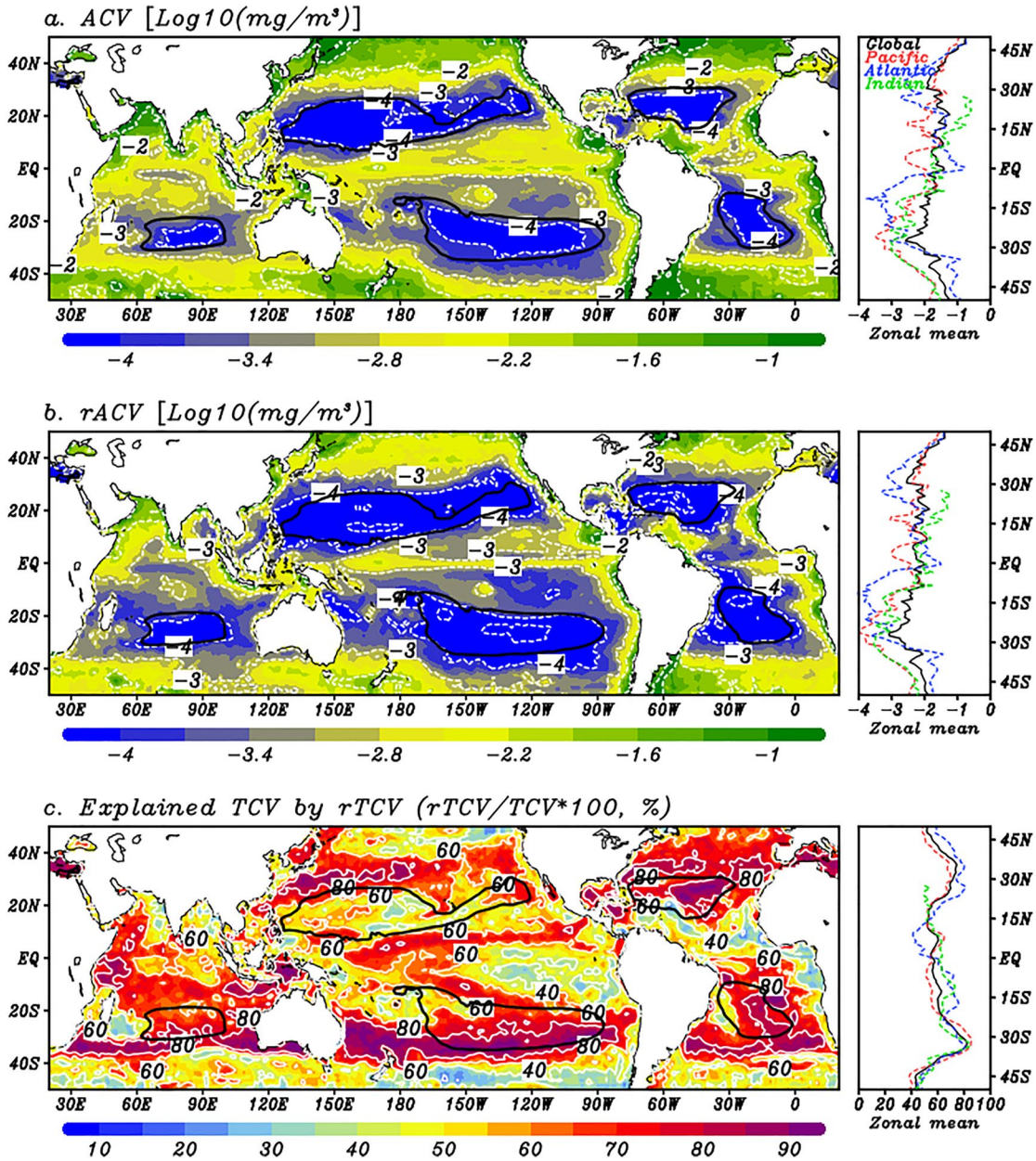

Figure 2. Climate-driven interannual variation subsequently contributes total chlorophyll variance (TCV) in the tropics. (a) Log_{10}-transformed anomalous chlorophyll variance (ACV) from September 1997 to August 2021 (Equation 4), (b) Log_{10}-transformed reconstructed ACV (rACV) obtained from reconstructed chlorophyll anomalies (rCHLa) using Multiple Linear Regression (MLR) method based on predictors in instantaneous and delayed climate effects (Equations 5 and 6), ACV and rACV are calculated in original scale of chlorophyll (mg/m^3) and then transformed to log_{10} to represent in global as shown in figures. (c) Explained TCV by rTCV (Equation 7). Black contour line denotes the edge of oligotrophic waters defined as below 0.07 mg/m^3 of mean annual chlorophyll.

seasonal component of TCV in the frontal regions between subtropical and subpolar gyres, adding interannual climate variability elevates the explained variance of TCV from 69.9% to 77.3% (+7.4%) in 35°S–25°S and from 59.5% to 71.3% (+11.8%) in 25°N–35°N. The general pattern of climate effects in GlobColour-AVM and ESA-OC-CCI-v5.0 (Figure S3 in Supporting Information S1) also represents the indispensable high contribution of climate-driven variability on TCV in the tropical oceans, compared to seasonal components only (Figure S2 in Supporting Information S1). rTCVs in GlobColour-AVM and ESA-OC-CCI-v5.0 are varied in regional scales but consistent in general within merging algorithms with the pattern of Glob-Colour-GSM result (Figure 2c).

21699291, 2022, 10, Downloaded from https://agupubs.onlinelibrary.wiley.com/doi/10.1029/2022JC019121, Wiley Online Library on [22/10/2022]. See the Terms and Conditions (https://onlinelibrary.wiley.com/terms-and-conditions) on Wiley Online Library for rules of use; OA articles are governed by the applicable Creative Commons License

3.3. Delayed Effects of Climate-Driven Variability on the Anomalous Chlorophyll Variability in the Tropical Oceans

The previous section attributed TCV explained by rTCV obtained from rCHL by considering metrics of both instantaneous and delayed effects in climate-driven variability. While the seasonal cycle contribute large portion of global TCV, rCHLa also contributes 26.3% of TCV in the tropical oceans. To explore the role of delayed effects on rCHLa, this section compares the ACC skill (Equation 8) between CHLa and rCHLa for two variants of the chlorophyll reconstruction: (a) A reconstruction that considers only instantaneous climate effects ($\tau = 0$ in Equation 5); (b) A reconstruction that includes both instantaneous and delayed climate effects ($\tau = 0 - 4$ in Equation 5).

The ACC skill of rCHLa using only instantaneous responses ($\tau = 0$ in Equation 5) shows a strong positive relationship in the tropical ocean, ACC = 0.63 averaged in 20°S–20°N (Figure 3a). rCHLa associated with instantaneous climate effects captures nearly half of the tropical chlorophyll variability with rCHLa timeseries correlations with CHLa of ACC = 0.64 in the Indian Ocean (40°E–100°E, 20°S–10°N) and ACC = 0.68 in the tropical Pacific Ocean (120°E–80°W, 20°S–20°N). Inspection of the instantaneous chlorophyll signals associated with each of the climate modes (left column of Figure 4) reveals that this arises primarily from ENSO and Pacific meridional mode (Di Lorenzo et al., 2013), with contributions from Atlantic (Grodsky et al., 2008) and Indian oceans (Park & Kug, 2013).

Adding delayed climate effects ($\tau = 0 - 4$ in Equation 5) elevates correlation skill (Figure 3b). The addition of delayed responses slightly increases the anomaly correlation between CHLa and rCHLa, from ACC = 0.63 to 0.67 in the tropical ocean, averaged in 20°S–20°N. We note that more marked impacts of the delayed climate variability are seen in the high correlation between CHLa and rCHLa in the off-equatorial Pacific and Indian Ocean, which was far more muted in the instantaneous response (Figure 3a). Delayed climate effects increase rCHLa skills (Figure 3c), from ACC = 0.64 to 0.72 in the Indian Ocean (40°E–100°E, 20°S–10°N), from ACC = 0.74 to 0.82 in off equatorial Northern Pacific (180°–90°W, 5°N–15°N), and ACC = 0.58 to 0.71 in the off equatorial Southern Pacific (160°W–90°W, 20°S–5°S).

rCHLa skill in the off-equatorial Pacific arise from ∼12 month delayed CHLa response to ENSO evolution (Figures 4a and 4b). ENSO-CHLa evolution is revealed as the principle components of tropical Pacific chlorophyll (Park et al., 2014) that evolve ENSO timescales across early summer to next summer (Hu et al., 2017) by oceanic and atmospheric drives of iron supply (Lim et al., 2022) and meridional nitrate advection in the off-equatorial Pacific (Ham et al., 2021). In addition, rCHLa skill in the Southern Indian Ocean is also related to ENSO evolution (Figures 4a and 4b). Jeon et al. (2022) demonstrated that wind stress forcing caused by ENSO to Indian Ocean teleconnections generates skillful chlorophyll prediction up to 2 years arise from off-equatorial Rossby waves and supplies nutrients in the Indian Ocean.

Skillfull rCHLa in the off-equatorial Pacific arise from ∼12 month delayed CHLa response to delayed effects of the North Pacific climate variabilities (Figures 4c and 4d), with moderate delayed effects of the Indian and Atlantic climate variabilities (Figures 4e–4h). North Pacific climate variability exerted a long-term influence on rCHLa. The slow transition in PDO has persistently influenced on rCHLa (Figure 4c). rCHLa estimated by NPGO has high ACC skill in the tropical Pacific up to 12 months (Figure 4d). NPGO evolves from initial SSTa locally in the North Pacific and is propagated to the tropical Pacific SSTa next year, which can initiate the central Pacific–ENSO and Pacific meridional mode–like patterns (Amaya, 2019; Di Lorenzo et al., 2015; Stuecker, 2018). rCHLa estimated by the Indian and Atlantic Oceans are relatively low correlation skill with CHLa beyond 6 months (Figures 4e–4h). In contrast, delayed ATL3 and AMM effects augment the tropical Pacific rCHLa, representing significant ACC skills against CHLa around a year after (Figures 4g and 4h). ATL3 and AMM SSTa variabilities in the Atlantic Ocean potentially trigger ENSO events a year later via atmospheric teleconnection of Gill-type Rossby-wave response (Ham, Kug, & Park, 2013; Park, Kug, et al., 2018) that may contribute rCHLa correlation skill for up to a year.

Reconciling such delayed effects of climate-driven variability onto rCHLa (Figure 3b) can provide rTCV skill in GlobColour-GSM (Figure 2c), which is consistent in rTCV skills in GlobColour-AVM and ESA-OC-CCI-v5.0 (Figure S3 in Supporting Information S1) elevated from the case considering the instantaneous climate-driven variability only (Figure S4 in Supporting Information S1). This result implies that delayed effects of climate-driven variability are indispensable components on explaining the contribution of TCV: temporal evolutions of ENSO (Lim et al., 2022; Park et al., 2011); the ENSO-Pacific meridional mode interaction (Di Lorenzo et al., 2013, 2015); and the pan-tropic interaction between ocean basins (Cai et al., 2019; Ham, Kug, & Park, 2013). The prominence of delayed effects also underpins the predictability of future chlorophyll fluctuations from the current climate state, which will be addressed in the next section.

21699291, 2022, 10, Downloaded from https://agupubs.onlinelibrary.wiley.com/doi/10.1029/2022JC019121, Wiley Online Library on [22/10/2022]. See the Terms and Conditions (https://onlinelibrary.wiley.com/terms-and-conditions) on Wiley Online Library for rules of use; OA articles are governed by the applicable Creative Commons License

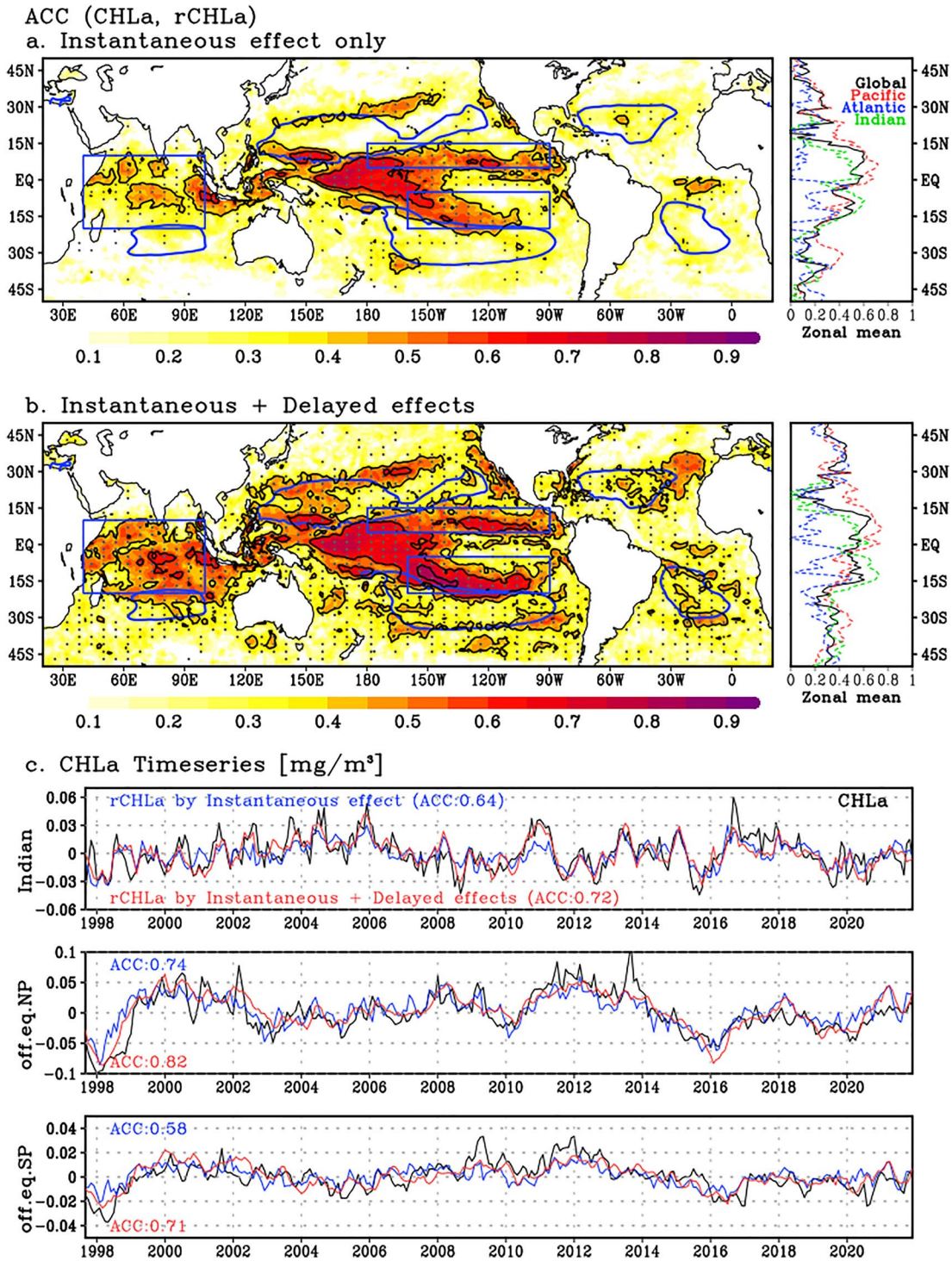

Figure 3. Reconstructions of chlorophyll anomalies (rCHLa) skills based on climate-driven variability. The spatial distribution of anomaly correlation coefficients (ACC) skill (anomalous correlation coefficients between CHLa and rCHLa; Equation 8). rCHLa is based on (a) instantaneous only ($\tau = 0$ in Equation 5) climate-driven variability, (b) both instantaneous and delayed effects ($\tau = 0 - 4$ in Equation 5) of climate-driven variability, and their zonal mean averaged ACC skills by latitude. Dots in spatial maps indicate the Student's *t*-test statistical significance at 99% confidence level. Black contour line denotes 0.4, 0.6, and 0.8 ACC skills. Blue contour line denotes the edge of oligotrophic waters defined as below 0.07 mg/m^3 of mean annual chlorophyll. (c) timeseries comparison of rCHLa between (a) (blue) and (b) (red) cases, and their ACC skills against rCHLa in the Indian Ocean (40°E–100°E, 20°S–10°N), off-equatorial Northern Pacific (180°–90°W, 5°N–15°N), and off-equatorial Southern Pacific (160°W–90°W, 20°S–5°S) defined by the boxes in blue.

21699291, 2022, 10, Downloaded from https://agupubs.onlinelibrary.wiley.com/doi/10.1029/2022JC019121, Wiley Online Library on [22/10/2022]. See the Terms and Conditions (https://onlinelibrary.wiley.com/terms-and-conditions) on Wiley Online Library for rules of use; OA articles are governed by the applicable Creative Commons License

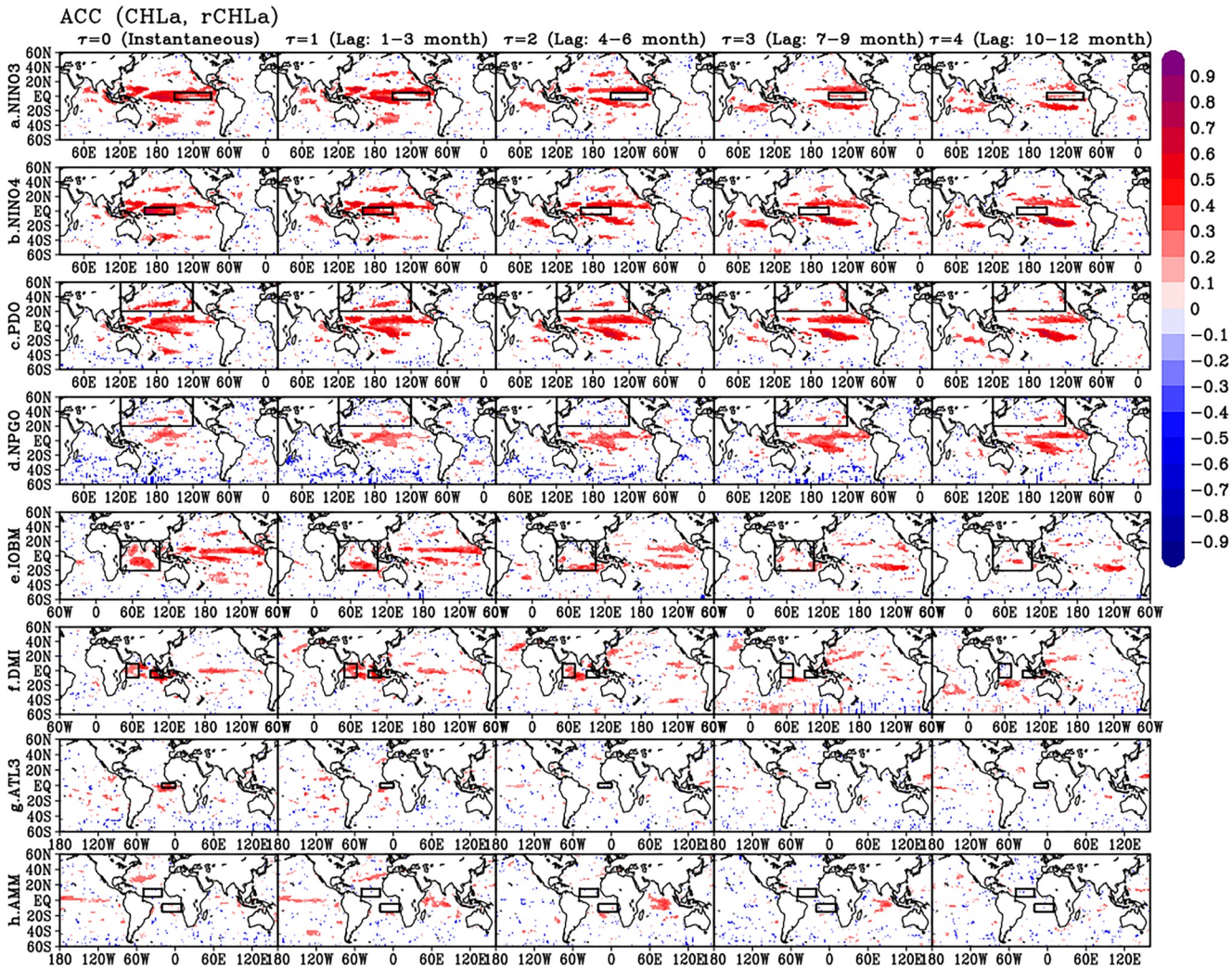

Figure 4. Anomaly correlation coefficients (ACC) skills between CHLa and rCHLa based on linear regression coefficients against each climate index of (a) NINO3, (b) NINO4, (c) PDO, (d) NPGO, (e) IOBM, (f) IOD, (g) ATL3, and (h) AMM depending on instantaneous ($\tau = 0$) or delayed time ($\tau = 1$ to 4) in GlobColour-GSM. Colors in figures indicate the Student's *t*-test statistical significance at 90% confidence level. Black boxes indicate the definition of regions for climate index as shown in Table 1. The longitude of each spatial map is centered on the region of climate indices (black box).

3.4. Statistical Predictability of Climate-Driven Chlorophyll Variability

In the previous section, we note that the evolution of climate-driven SSTa variability and its delayed effect from prior seasons are able to reconstruct surface chlorophyll in many ocean regions. This section quantifies the capacity of these same climate modes to anticipate future chlorophyll changes. In this section, rCHLa_predic is generated by empirical relationship between observed CHLa and the delayed effects of climate-driven SSTa variability up to 4 seasons in advance ($\tau = 1$ to $\tau = 4$) with stepwise removal of delayed effects of climate depending on lead times and without the information of instantaneous effects of climate ($\tau = 0$) in the spatio-temporal grid cells (Table S1 in Supporting Information S1).

The delayed response to climate variability yields skillful seasonal rCHLa_predic for some tropical regions (Figure 5). The spatially-resolved ACC_predic (Equation 9) for 2 month lead time shows overall predictability skills of ACC_predic = 0.63 in the tropical ocean (Figure 5a). In particular, the tropical Pacific (ACC_predic = 0.67) and Indian (ACC_predic = 0.60) Oceans are highly predictable, which is consistent pattern in ACC_predic skills of GlobColour-AVM (0.77, 0.58), ESA-OC-CCI-v5.0 (0.70, 0.69), and ensemble mean of all satellite datasets (0.73, 0.64) in the tropical Pacific and Indian Oceans, respectively (Figure S5 in Supporting Information S1).

21699291, 2022, 10, Downloaded from https://agupubs.onlinelibrary.wiley.com/doi/10.1029/2022JC019121, Wiley Online Library on [22/10/2022]. See the Terms and Conditions (https://onlinelibrary.wiley.com/terms-and-conditions) on Wiley Online Library for rules of use; OA articles are governed by the applicable Creative Commons License

The delayed effects of climate-driven variability from 6 month lead time also show promising multiple season predictability (Figure 5b), with correlation between observed and predicted chloropyll maintained at ACC_predic = 0.51 in the tropical ocean, ACC_predic = 0.59 in the tropical Pacific, and ACC_predic = 0.43 in the Indian Ocean.

We further decompose regional ACC_predic skills in each calendar month (Figures 5c–5e). The off-equatorial Pacific CHLa (Figures 5c and 5d) are strongly predictable during seasonal to multi-annual timescales, related to ENSO and Pacific meridional mode interactions (Figures 4a–4d) with marginal contributions of Indian and Atlantic modes (Figures 4e–4h). In particular, CHLa in the off-equatorial northern Pacific is mostly predictable

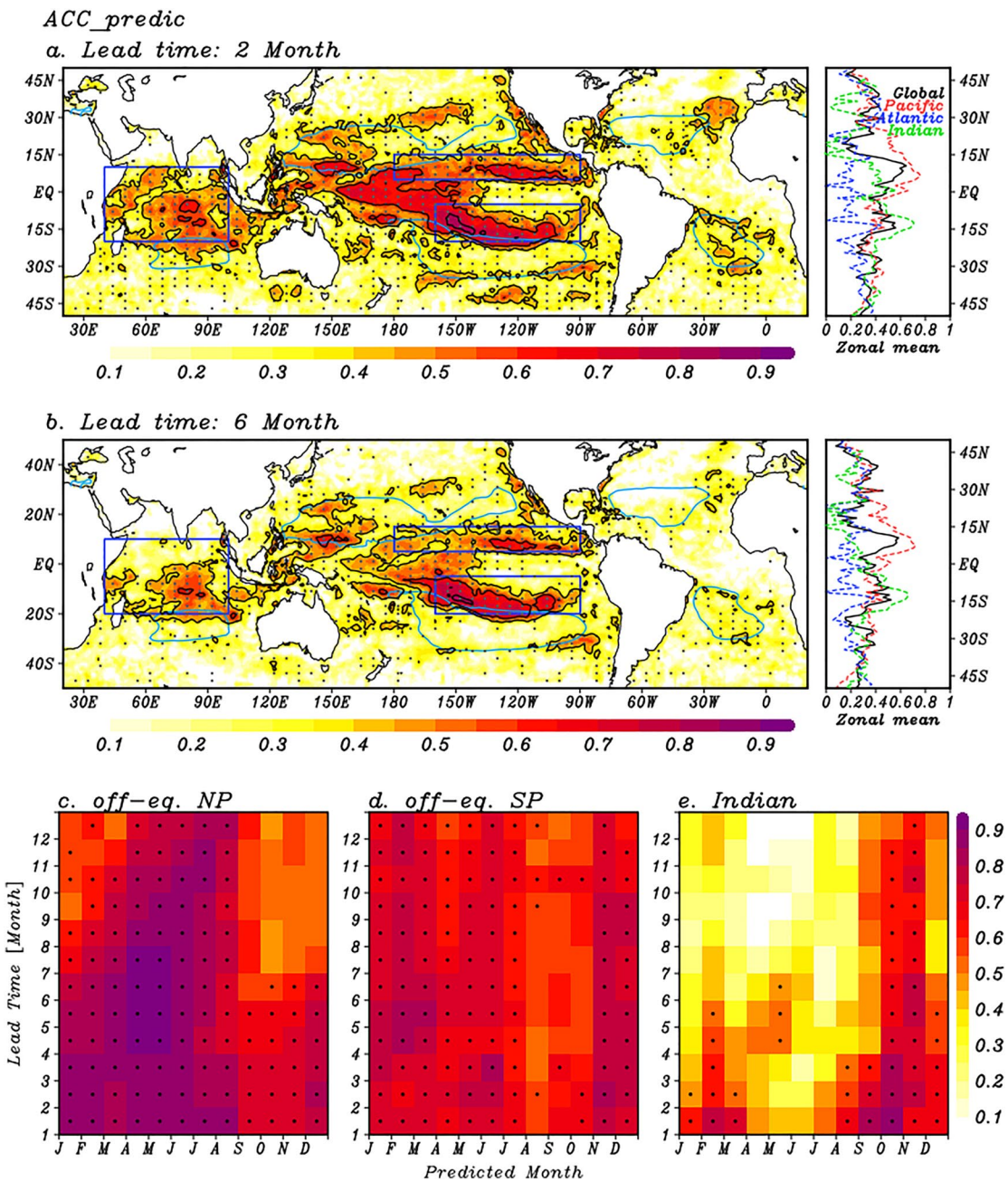

Figure 5. Spatially resolved ACC_predic (Equation 9) skills of rCHLa_predic based on delayed effects of climate-driven variability. rCHLa_predic is based on (a) average of 1–3 month lead times, (b) average of 5–7 month lead times in climate-driven variability. Skyblue contour line denotes the edge of oligotrophic waters defined as below 0.07 mg/m^3 of mean annual chlorophyll. ACC_predic skills as a function of month (*x* axis) and lead time (*y* axis) in (c) off-equatorial Northern Pacific (180°–90°W, 5°N–15°N), (d) off-equatorial Southern Pacific (160°W–90°W, 20°S–5°S) and (e) Indian Ocean (40°E–100°E, 20°S–10°N). Dots in figures indicate the Student's *t*-test statistical significance at 99% confidence level.

21699291, 2022, 10, Downloaded from https://agupubs.onlinelibrary.wiley.com/doi/10.1029/2022JC019121, Wiley Online Library on [22/10/2022]. See the Terms and Conditions (https://onlinelibrary.wiley.com/terms-and-conditions) on Wiley Online Library for rules of use; OA articles are governed by the applicable Creative Commons License

from winter to summer (Figure 5c), which may be strongly connected with low-frequency ENSO and Pacific meridional mode (Di Lorenzo et al., 2015) as shown in its low-frequency fluctuations of time series (middle panel of Figure 3c). In addition, long-term delayed effects of ENSO and North Pacific climate variabilities influence CHLa in the Indian Ocean CHLa beyond 6 months (Figures 4a–4c) that elevate ACC_predic skill in the early boreal winter season from October to November (Figure 5e).

4. Summary

The present study revisited previous works by assessing chlorophyll variance and its subsequent decomposition into seasonal and climate drivers based on the last 24 years of satellite chlorophyll. We find that the first-order contribution of the seasonal cycle dominates zonal bands of chlorophyll variance in the midlatitudes at the front between subtropical and subpolar gyres, locally maximized at 59.5% of variance in 25°N–35°N and 69.9% in 35°S–25°S (Figure 1c).

In addition, we showed that the combination of the seasonal cycle and climate-driven variability (instantaneous + delayed effects) explains considerable chlorophyll variances in the tropical ocean 20°N–20°S of 57.2% (Figure 2c). This value is +26.3% greater than the explained variance by seasonal cycle solely (30.9%) (Figure 1c). The elevation of explained TCV in the tropical ocean basins can be achieved from reconciling multi-seasonal delayed effects of eight modes of climate variability onto CHLa.

We demonstrated that delayed climate effects elevates rCHLa skill (Figure 3b). The addition of delayed responses remarkably impacts on rCHLa skills in the off-equatorial Pacific and Indian Ocean, which was far more muted in the instantaneous response only (Figure 3a). Delayed climate effects increase correlation skills of rCHLa time-series (Figure 3c), from ACC = 0.64 to 0.72 in the Indian Ocean (40°E–100°E, 20°S–10°N), from ACC = 0.74 to 0.82 in off equatorial Northern Pacific (180°–90°W, 5°N–15°N), and ACC = 0.58 to 0.71 in the off equatorial Southern Pacific (160°W–90°W, 20°S–5°S).

The schematic in Figure 6 shows the major sources of global chlorophyll variation: 41.6% from Seasonal cycle only (Case 1), 49.1% from both seasonal cycle and instantaneous climate modes (Case 2), and 61.1% from all seasonal cycle, instantaneous and delayed climate modes (Case 3).

The implication of this study is that delayed climate effects can provide a source of chlorophyll predictability in the tropical oceans (Figure 5). The spatially-resolved ACC_predic skill between CHLa and rCHLa_predic that observed for 2 month lead time shows overall predictability skills of ACC_predic = 0.63 in the tropical ocean (Figure 5a). In particular, the tropical Pacific (ACC_predic = 0.67) and Indian (ACC_predic = 0.60) Oceans are highly predictable. The delayed effects of climate-driven variability from 6 month lead time also shows promising multiple season predictability (Figure 5b), with ACC_predic skill between CHLa and rCHLa_predic maintained at ACC_predic = 0.51 in the tropical ocean, ACC_predic = 0.59 in the tropical Pacific, and ACC_predic = 0.43 in the Indian Ocean.

5. Discussion

The spatio-temporal variations of satellite ocean color estimates of chlorophyll concentration have informed the role of variations of the physical environment in the marine phytoplankton changes with the availability of merged products combining algorithms of several satellite generations (Chavez et al., 1999, 2011; Di Lorenzo et al., 2008, 2013; Gorgues et al., 2010; Grodsky et al., 2008; Lim et al., 2022; Murtugudde et al., 1999; Park, Dunne, & Stock, 2018; Polovina et al., 2017; Tian et al., 2021; Vantrepotte & Mélin, 2009; Yoder & Kennelly, 2003; Zhang et al., 2018). We demonstrate that the climate variability defined by SSTa in ocean basins can provide a source of long-term chlorophyll predictability. In some cases, influences within an ocean basin combine with remote influences between ocean basins via atmospheric teleconnections (Alexander et al., 2002; Amaya, 2019; Cai et al., 2019; Capotondi et al., 2015; Di Lorenzo et al., 2010; Ham, Kug, Park, et al., 2013; Hong et al., 2022; Jacox et al., 2022; Kug & Kang, 2006; Park, Kug, et al., 2018; Tian et al., 2021; Timmermann et al., 2018; Vimont et al., 2003; Yeh et al., 2018). The fidelity of simulating the climate-driven SSTa variability in the earth system model may be further required to achieve the longer horizon of marine ecosystem predictability (Frölicher et al., 2020; Séférian et al., 2014; Taboada et al., 2019) and seasonal to multi-annual prediction skill (Ham et al., 2021; Ilyina et al., 2021; Park et al., 2019; Rousseaux et al., 2021; Rousseaux & Gregg, 2017).

21699291, 2022, 10, Downloaded from https://agupubs.onlinelibrary.wiley.com/doi/10.1029/2022JC019121, Wiley Online Library on [22/10/2022]. See the Terms and Conditions (https://onlinelibrary.wiley.com/terms-and-conditions) on Wiley Online Library for rules of use; OA articles are governed by the applicable Creative Commons License

The statistical predictability results in the present study, built upon the demonstrated importance of time evolution of climate variability by comparing two approaches of rTCV between including delayed effects (Figure 2c and Figure S3 in Supporting Information S1) or disregarding them (Figure S4 in Supporting Information S1), suggests promising avenues for marine ecosystem prediction in the tropical Pacific and Indian Oceans. One weakness of the present approach is only considered by SSTa based climate indices that could be improved by considering physical and biogeochemical reemergences from subsurface to the surface (Frölicher et al., 2020; Park et al., 2019; Séférian et al., 2014). Such potential predictors based on subsurface components may improve the present predictability skills as well as the upper ocean heat content that is a part of critical initialization components on dynamical ENSO prediction model (Smith, 1995; Zebiak & Cane, 1987). Physical climate can also potentially extend the predictability horizon of ocean color based estimates for oceanic net primary production in off-equatorial Pacific oceans (Taboada et al., 2019) that may include delayed effects of climate variability as shown in the present work for CHLa predictability.

It has been reported that global marine chlorophyll is declining (Behrenfeld et al., 2006; Boyce et al., 2014; Henson et al., 2010; Polovina et al., 2008). We note that linear trends of 24-years of satellite ocean color in the tropical and midlatitude oceans are regionally diverse depending on merging algorithms (Figure S1 in Supporting Information S1). While GlobColour-GSM and GlobColour-AVM exhibits negative trends of chlorophyll within

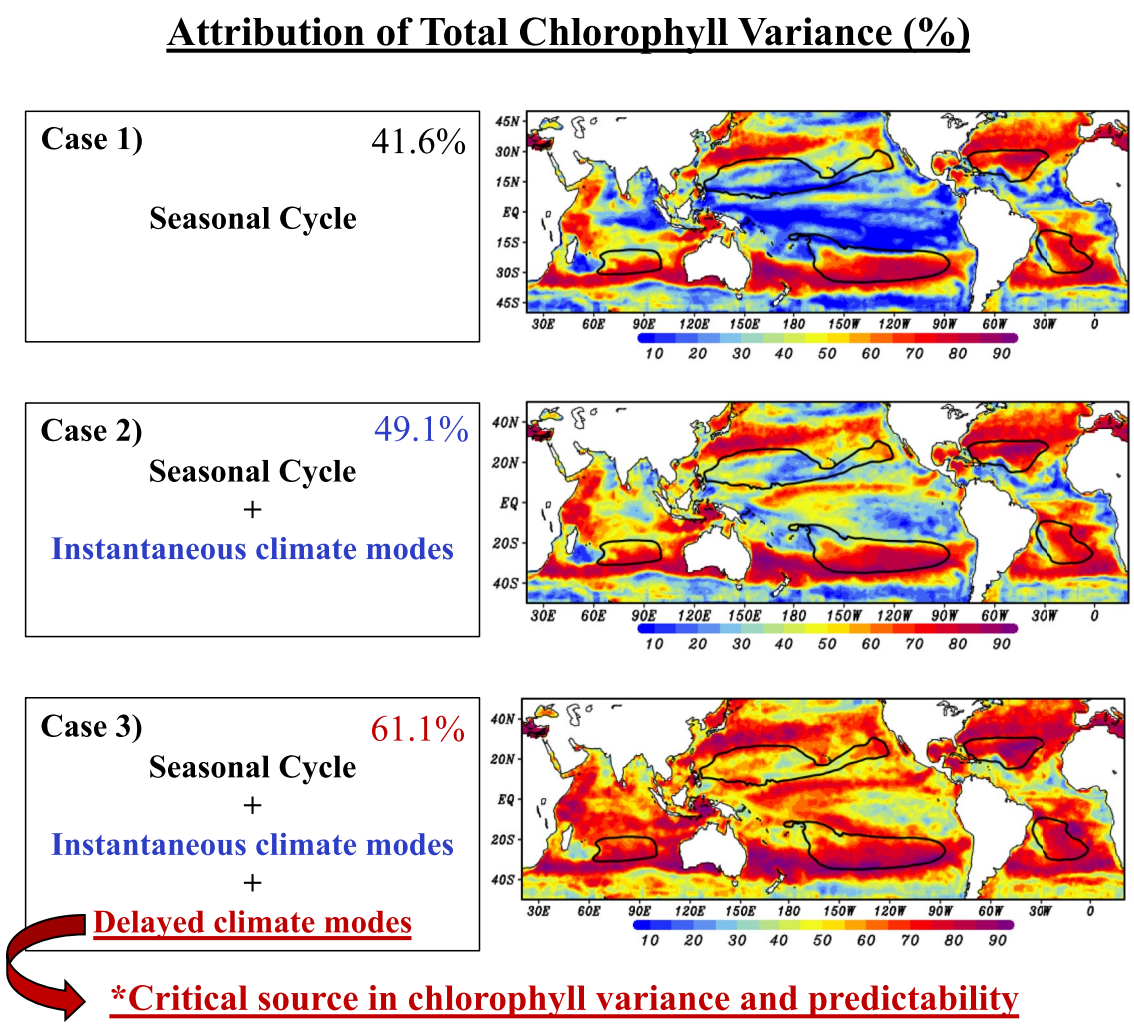

Figure 6. Schematic figure for the summary of the present study. The source of total chlorophyll variation (TCV): 41.6% from seasonal cycle only (Case 1), 49.1% from both seasonal cycle and instantaneous climate modes (Case 2), and 61.1% from all seasonal cycle, instantaneous and delayed climate modes (Case 3). All cases of figures are based on GlobColour-GSM (Case 1: Figure 1c, Case 2: Figure S4a in Supporting Information S1, Case 3: Figure 2c). Black contour line denotes the edge of oligotrophic waters defined as below 0.07 mg/m^3 of mean annual chlorophyll.

21699291, 2022, 10, Downloaded from https://agupubs.onlinelibrary.wiley.com/doi/10.1029/2022JC019121, Wiley Online Library on [22/10/2022]. See the Terms and Conditions (https://onlinelibrary.wiley.com/terms-and-conditions) on Wiley Online Library for rules of use; OA articles are governed by the applicable Creative Commons License

Table 2
Area of Oligotrophic Waters by Removing the Seasonal Cycle Estimated in GlobColour-GSM, AVM, and ESA-OC-CCI-v5.0 With Previous Report Polovina et al. (2008) Calculation

Ocean	1998 mean area, 10^6 km^2	Increase in area, 10^6 km^2/yr,	*p*-value
North Pacific	GSM: 11.53, AVM: 21.93, ESA: 18.71, P08: 16.22	GSM: 0.68, AVM: 0.23, ESA:0.15, P08: 0.35	GSM:0.032, AVM:0.070, ESA:0.17, P08:2.48^{-08}
South Pacific	GSM: 14.59, AVM: 22.92, ESA: 18.88 P08: 18.04	GSM: 0.18, AVM:-0.04, ESA:-0.08, P08: 0.25	GSM:0.13, AVM: 0.41, ESA:0.11, P08:1.47^{-06}
North Atlantic	GSM: 5.23, AVM: 5.78, ESA: 6.20 P08: 4.01	GSM: 0.16, AVM:0.06, ESA:0.01, P08:0.17	GSM:0.060, AVM:0.18, ESA:0.58, P08:1.41^{-09}
South Atlantic	GSM: 5.02, AVM: 7.47, ESA: 6.44 P08: 6.10	GSM:0.10, AVM:0.002, ESA:-0.05, P08:0.05	GSM:0.077, AVM:0.93, ESA:0.11, P08:2.61^{-02}
Total areas	GSM: 36.92, AVM: 60.08, ESA: 51.28 P08: 44.38	GSM:1.15, AVM:0.25, ESA:0.05, P08:0.82	GSM:0.067, AVM:0.21, ESA:0.66, P08: N/A

Note. Each value of oligotrophic water areas calculated from different datasets is denoted with acronym GSM, AVM, ESA, and P08 (i.e., Polovina et al., 2008).

30°N–30°S (Figures S1a and S1b in Supporting Information S1), ESA-OC-CCI-v5.0 shows a somewhat mixed pattern of negative and positive trends in 30°N–30°S and strong positive trends in high latitudes beyond 30° of both hemispheres (Figure S1c in Supporting Information S1). In addition, Polovina et al. (2008) pointed out the expansion of oligotrophic waters from 1998 through 2006 using an early 9-year timeseries of SeaWiFS. We revisited the areal extent of oligotrophic water using 24-year timeseries of all datasets including seasonal cycles (Figure S6 in Supporting Information S1). Variations of oligotrophic water area represent a good agreement of first-order contributions of the seasonal cycle in all datasets. However, deseasonalized trends of oligotrophic water areas are diverse with noticeable expansion in GlobColour-GSM while insignificant expansion in GlobColour-AVM and ESA-OC-CCI-v5.0 (Table 2), supporting the result that all data sets to provide a consistent contribution of the seasonal cycle contribution on TCV in the present study despite of their inconsistency of linear trends.

The remaining question unanswered in the present TCV analysis is what other mechanisms may drive the currently "unexplained" spatio-temporal TCV as shown in the residual of explained TCV by rTCV (Figure S7 in Supporting Information S1). These unanswered sources in TCV may constitute a quarter of midlatitude variability and nearly less than half of the tropical variabilities (Figure S7 in Supporting Information S1). Potential sources of explanation go far beyond the simple physical climate metrics discussed in the present work and include previously identified mechanisms such as: internal dynamics of biogeochemical and ecological cycling on zooplankton grazing pressures on phytoplankton (Gorgues et al., 2010; Tian et al., 2021); anomalous phytoplankton blooms driven by volcanic ash increases in iron supply (Achterberg et al., 2013; Hamme et al., 2010); high contribution of the Amazon and Orinoco river plumes into the tropical Atlantic (Grodsky et al., 2008); widespread phytoplankton blooms triggered by Australian wild fires in the Southern Pacific (Tang et al., 2021); diversity and asymmetry of ENSO (Lee et al., 2014; Park et al., 2014); ENSO-driven freshwater flux (Tian et al., 2020); nonlinearity of horizontal nitrate advection (Ham et al., 2021); nonlinear statistical approach (Martinez et al., 2020); and tropical instability wave driven nutrient supply (Evans et al., 2009) in the tropical Pacific phytoplankton variation.

6. Conclusion

Successful achievements of climate prediction systems reflect long term investments in the observational evaluations and model developments onto next generation marine ecosystem prediction systems. This work takes advantage of the multi-decade satellite chlorophyll record to characterize variability and demonstrates that delayed effects of sea surface temperature from prior seasons improve model estimates of chlorophyll in the equatorial Pacific and Indian Oceans. Our results point to several directions to better constrain regional discrepancies and the importance of both the seasonal cycle and interannual variation of chlorophyll to understand interactions between climate and marine ecosystem as observed by satellites and simulated in earth system models. Along with developments for comprehensive marine biogeochemical dynamics (Séférian et al., 2020), the achievements of dynamical Earth system modeling development efforts are illustrated with the growing the fidelity to better benchmarks of the mean state climate system. ENSO for example, (Planton et al., 2021), appears to provide a promising avenue for better predictions of the marine ecosystem with application for living resources management (Tommasi et al., 2017) because of its close connection between climate and chlorophyll variability.

21699291, 2022, 10, Downloaded from https://agupubs.onlinelibrary.wiley.com/doi/10.1029/2022JC019121, Wiley Online Library on [22/10/2022]. See the Terms and Conditions (https://onlinelibrary.wiley.com/terms-and-conditions) on Wiley Online Library for rules of use; OA articles are governed by the applicable Creative Commons License

Our analysis with satellite ocean color demonstrates a key role of delayed effects of physical climate variability strongly on chlorophyll variance that may provide a key source of marine ecosystem predictability in the Earth system model.

Data Availability Statement

GlobColour version 2021.1 merged by Garver, Siegel, Maritorena model (GlobColour-GSM) and merged by the simple average method model (GlobColour-AVM) are available online https://hermes.acri.fr or https://www.globcolour.info. European Space Agency Ocean Colour Climate Change Initiative project version 5.0 (ESA-OC-CCI-v5.0) is available online https://climate.esa.int/en/projects/ocean-colour/. NOAA Extended Reconstructed SST version 5 (ERSST v5) is available online https://psl.noaa.gov/data/gridded/data.noaa.ersst.v5.html.

Acknowledgments
The authors thank fruitful discussions about chlorophyll anomalies related to the North Pacific climate with Youngji Joh (Princeton University-AOS) and related to the Atlantic Ocean climate with Sang-Ki Lee (NOAA-AOML). The authors also thank Colleen M. Petrik (University of California San Diego), Elizabeth J. Drenkard (NOAA-GFDL), and Graeme MacGilchrist (Princeton University-AOS) for providing earlier reviews of our results and appreciate valuable comments for elevating the quality of the manuscript from two anonymous reviewers. H.-G. Lim is supported under award NA18OAR4320123 from the National Oceanic and Atmospheric Administration, U.S. Department of Commerce. The statements, findings, conclusions, and recommendations are those of the author(s) and do not necessarily reflect the views of the National Oceanic and Atmospheric Administration, or the U.S. Department of Commerce.

References

Achterberg, E. P., Moore, C. M., Henson, S. A., Steigenberger, S., Stohl, A., Eckhardt, S., et al. (2013). Natural iron fertilization by the Eyjafjallajökull volcanic eruption. *Geophysical Research Letters*, *40*(5), 921–926. https://doi.org/10.1002/grl.50221

Alexander, M. A., Bladé, I., Newman, M., Lanzante, J. R., Lau, N.-C., & Scott, J. D. (2002). The atmospheric bridge: The influence of ENSO teleconnections on air–sea interaction over the global oceans. *Journal of Climate*, *15*(16), 2205–2231. https://doi.org/10.1175/1520-0442(2002)015<2205:tabtio>2.0.co;2

Amaya, D. J. (2019). The Pacific meridional mode and ENSO: A review. *Current Climate Change Reports*, *5*(4), 296–307. https://doi.org/10.1007/s40641-019-00142-x

Ardyna, M., Babin, M., Gosselin, M., Devred, E., Rainville, L., & Tremblay, J. É. (2014). Recent Arctic Ocean sea ice loss triggers novel fall phytoplankton blooms. *Geophysical Research Letters*, *41*(17), 6207–6212. https://doi.org/10.1002/2014gl061047

Arrigo, K. R. (2003). Phytoplankton dynamics within 37 Antarctic coastal polynya systems. *Journal of Geophysical Research*, *108*(C8), 3271. https://doi.org/10.1029/2002jc001739

Banse, K. (1992). Grazing, temporal changes of phytoplankton concentrations, and the microbial loop in the open sea. In P. G. Falkowski, A. D. Woodhead, & K. Vivirito (Eds.), *Primary productivity and biogeochemical cycles in the sea* (pp. 409–440). Springer US. https://doi.org/10.1007/978-1-4899-0762-2_22

Behrenfeld, M. J., O'Malley, R. T., Siegel, D. A., McClain, C. R., Sarmiento, J. L., Feldman, G. C., et al. (2006). Climate-driven trends in contemporary ocean productivity. *Nature*, *444*(7120), 752–755. https://doi.org/10.1038/nature05317

Behrenfeld, M. J., Randerson, J. T., McClain, C. R., Feldman, G. C., Los, S. O., Tucker, C. J., et al. (2001). Biospheric primary production during an ENSO transition. *Science*, *291*(5513), 2594–2597. https://doi.org/10.1126/science.1055071

Bond, N. A., Overland, J. E., Spillane, M., & Stabeno, P. (2003). Recent shifts in the state of the North Pacific. *Geophysical Research Letters*, *30*(23), 2183. https://doi.org/10.1029/2003GL018597

Boyce, D. G., Dowd, M., Lewis, M. R., & Worm, B. (2014). Estimating global chlorophyll changes over the past century. *Progress in Oceanography*, *122*, 163–173. https://doi.org/10.1016/j.pocean.2014.01.004

Cai, W., Wu, L., Lengaigne, M., Li, T., McGregor, S., Kug, J. S., et al. (2019). Pantropical climate interactions. *Science*, *363*(6430), eaav4236. https://doi.org/10.1126/science.aav4236

Capotondi, A., Wittenberg, A. T., Newman, M., Di Lorenzo, E., Yu, J. Y., Braconnot, P., et al. (2015). Understanding ENSO diversity. *Bulletin of the American Meteorological Society*, *96*(6), 921–938. https://doi.org/10.1175/BAMS-D-13-00117.1

Carr, M.-E., Friedrichs, M. A., Schmeltz, M., Noguchi Aita, M., Antoine, D., Arrigo, K. R., et al. (2006). A comparison of global estimates of marine primary production from ocean color. *Deep Sea Research Part II: Topical Studies in Oceanography*, *53*(5), 741–770. https://doi.org/10.1016/j.dsr2.2006.01.028

Chassot, E., Bonhommeau, S., Dulvy, N. K., Mélin, F., Watson, R., Gascuel, D., & Le Pape, O. (2010). Global marine primary production constrains fisheries catches. *Ecology Letters*, *13*(4), 495–505. https://doi.org/10.1111/j.1461-0248.2010.01443.x

Chavez, F., Strutton, P., Friederich, G., Feely, R., Feldman, G., Foley, D., & McPhaden, M. (1999). Biological and chemical response of the equatorial Pacific Ocean to the 1997-98 El Niño. *Science*, *286*(5447), 2126–2131. https://doi.org/10.1126/science.286.5447.2126

Chavez, F. P., Messié, M., & Pennington, J. T. (2011). Marine primary production in relation to climate variability and change. *Annual Review of Marine Science*, *3*(1), 227–260. https://doi.org/10.1146/annurev.marine.010908.163917

Cheung, W. W., Lam, V. W., Sarmiento, J. L., Kearney, K., Watson, R., Zeller, D., & Pauly, D. (2010). Large-scale redistribution of maximum fisheries catch potential in the global ocean under climate change. *Global Change Biology*, *16*(1), 24–35. https://doi.org/10.1111/j.1365-2486.2009.01995.x

Dave, A. C., Barton, A. D., Lozier, M. S., & McKinley, G. A. (2015). What drives seasonal change in oligotrophic area in the subtropical North Atlantic? *Journal of Geophysical Research: Oceans*, *120*, 3958–3969. https://doi.org/10.1002/2015JC010787

Di Lorenzo, E., Cobb, K. M., Furtado, J. C., Schneider, N., Anderson, B. T., Bracco, A., et al. (2010). Central Pacific El Niño and decadal climate change in the North Pacific Ocean. *Nature Geoscience*, *3*(11), 762–765. https://doi.org/10.1038/ngeo984

Di Lorenzo, E., Combes, V., Keister, J. E., Strub, P. T., Thomas, A. C., Franks, P. J., et al. (2013). Synthesis of Pacific Ocean climate and ecosystem dynamics. *Oceanography*, *26*(4), 68–81. https://doi.org/10.5670/oceanog.2013.76

Di Lorenzo, E., Liguori, G., Schneider, N., Furtado, J., Anderson, B., & Alexander, M. (2015). ENSO and meridional modes: A null hypothesis for Pacific climate variability. *Geophysical Research Letters*, *42*(21), 9440–9448. https://doi.org/10.1002/2015gl066281

Di Lorenzo, E., Schneider, N., Cobb, K. M., Franks, P. J. S., Chhak, K., Miller, A. J., et al. (2008). North Pacific Gyre Oscillation links ocean climate and ecosystem change. *Geophysical Research Letters*, *35*(8), L08607. https://doi.org/10.1029/2007GL032838

Doi, T., Tozuka, T., & Yamagata, T. (2010). The Atlantic meridional mode and its coupled variability with the Guinea Dome. *Journal of Climate*, *23*(2), 455–475. https://doi.org/10.1175/2009jcli3198.1

Dunne, J. P., Sarmiento, J. L., & Gnanadesikan, A. (2007). A synthesis of global particle export from the surface ocean and cycling through the ocean interior and on the seafloor. *Global Biogeochemical Cycles*, *21*(4), GB4006. https://doi.org/10.1029/2006gb002907

21699291, 2022, 10, Downloaded from https://agupubs.onlinelibrary.wiley.com/doi/10.1029/2022JC019121, Wiley Online Library on [22/10/2022]. See the Terms and Conditions (https://onlinelibrary.wiley.com/terms-and-conditions) on Wiley Online Library for rules of use; OA articles are governed by the applicable Creative Commons License

Dutkiewicz, S., Hickman, A. E., Jahn, O., Henson, S., Beaulieu, C., & Monier, E. (2019). Ocean colour signature of climate change. *Nature Communications*, *10*(1), 578. https://doi.org/10.1038/s41467-019-08457-x

Dutkiewicz, S., Mouw, C. B., Rousseaux, C. S., Stock, C., Ciavatta, S., Baird, M., et al. (2020). Synergy between ocean colour and biogeochemical/ecosystem models. In *International Ocean Colour Coordinating Group Report Series No. 19*.

Evans, W., Strutton, P. G., & Chavez, F. P. (2009). Impact of tropical instability waves on nutrient and chlorophyll distributions in the equatorial Pacific. *Deep Sea Research Part I: Oceanographic Research Papers*, *56*(2), 178–188. https://doi.org/10.1016/j.dsr.2008.08.008

Everett, J. D., Baird, M. E., Roughan, M., Suthers, I. M., & Doblin, M. A. (2014). Relative impact of seasonal and oceanographic drivers on surface chlorophyll a along a Western Boundary Current. *Progress in Oceanography*, *120*, 340–351. https://doi.org/10.1016/j.pocean.2013.10.016

Falkowski, P. G. (1994). The role of phytoplankton photosynthesis in global biogeochemical cycles. *Photosynthesis Research*, *39*(3), 235–258. https://doi.org/10.1007/bf00014586

Falkowski, P. G., & Woodhead, A. D. (2013). *Primary productivity and biogeochemical cycles in the sea*. Springer Science & Business Media.

Fennel, K., Gehlen, M., Brasseur, P., Brown, C. W., Ciavatta, S., Cossarini, G., et al. (2019). Advancing marine biogeochemical and ecosystem reanalyses and forecasts as tools for monitoring and managing ecosystem health. *Frontiers in Marine Science*, *6*, 89. https://doi.org/10.3389/fmars.2019.00089

Friedland, K. D., Stock, C., Drinkwater, K. F., Link, J. S., Leaf, R. T., Shank, B. V., et al. (2012). Pathways between primary production and fisheries yields of large marine ecosystems. *PLoS One*, *7*(1), e28945. https://doi.org/10.1371/journal.pone.0028945

Frölicher, T. L., Ramseyer, L., Raible, C. C., Rodgers, K. B., & Dunne, J. (2020). Potential predictability of marine ecosystem drivers. *Biogeosciences*, *17*(7), 2061–2083. https://doi.org/10.5194/bg-17-2061-2020

Gorgues, T., Menkes, C., Slemons, L., Aumont, O., Dandonneau, Y., Radenac, M. H., et al. (2010). Revisiting the La Niña 1998 phytoplankton blooms in the equatorial Pacific. *Deep Sea Research Part I: Oceanographic Research Papers*, *57*(4), 567–576. https://doi.org/10.1016/j.dsr.2009.12.008

Grodsky, S. A., Carton, J. A., & McClain, C. R. (2008). Variability of upwelling and chlorophyll in the equatorial Atlantic. *Geophysical Research Letters*, *35*(3), L03610. https://doi.org/10.1029/2007GL032466

Ham, Y.-G., Joo, Y.-S., & Park, J.-Y. (2021). Mechanism of skillful seasonal surface chlorophyll prediction over the southern Pacific using a global Earth system model. *Climate Dynamics*, *56*(1), 45–64. https://doi.org/10.1007/s00382-020-05403-2

Ham, Y.-G., Kug, J.-S., & Park, J.-Y. (2013). Two distinct roles of Atlantic SSTs in ENSO variability: North tropical Atlantic SST and Atlantic Niño. *Geophysical Research Letters*, *40*(15), 4012–4017. https://doi.org/10.1002/grl.50729

Ham, Y.-G., Kug, J.-S., Park, J.-Y., & Jin, F.-F. (2013). Sea surface temperature in the north tropical Atlantic as a trigger for El Niño/Southern Oscillation events. *Nature Geoscience*, *6*(2), 112–116. https://doi.org/10.1038/ngeo1686

Hamme, R. C., Webley, P. W., Crawford, W. R., Whitney, F. A., DeGrandpre, M. D., Emerson, S. R., et al. (2010). Volcanic ash fuels anomalous plankton bloom in subarctic northeast Pacific. *Geophysical Research Letters*, *37*(19), L19604. https://doi.org/10.1029/2010GL044629

Hazen, E. L., Scales, K. L., Maxwell, S. M., Briscoe, D. K., Welch, H., Bograd, S. J., et al. (2018). A dynamic ocean management tool to reduce bycatch and support sustainable fisheries. *Science Advances*, *4*(5), eaar3001. https://doi.org/10.1126/sciadv.aar3001

Henson, S. A., Dunne, J. P., & Sarmiento, J. L. (2009). Decadal variability in North Atlantic phytoplankton blooms. *Journal of Geophysical Research*, *114*, C04013. https://doi.org/10.1029/2008JC005139

Henson, S. A., Sanders, R., & Madsen, E. (2012). Global patterns in efficiency of particulate organic carbon export and transfer to the deep ocean. *Global Biogeochemical Cycles*, *26*(1), GB1028. https://doi.org/10.1029/2011GB004099

Henson, S. A., Sarmiento, J. L., Dunne, J. P., Bopp, L., Lima, I. D., Doney, S. C., et al. (2010). Detection of anthropogenic climate change in satellite records of ocean chlorophyll and productivity.

Hong, C.-C., Li, T., LinHo, & Chen, Y.-C. (2010). Asymmetry of the Indian Ocean basinwide SST anomalies: Roles of ENSO and IOD. *Journal of Climate*, *23*(13), 3563–3576. https://doi.org/10.1175/2010jcli3320.1

Hong, J.-S., Yeh, S.-W., & Yang, Y.-M. (2022). Interbasin interactions between the Pacific and Atlantic Oceans depending on the phase of Pacific decadal oscillation and Atlantic multidecadal oscillation. *Journal of Climate*, *35*(9), 2883–2894. https://doi.org/10.1175/jcli-d-21-0408.1

Hu, Z.-Z., Kumar, A., Huang, B., Zhu, J., Zhang, R.-H., & Jin, F.-F. (2017). Asymmetric evolution of El Niño and La Niña: The recharge/discharge processes and role of the off-equatorial sea surface height anomaly. *Climate Dynamics*, *49*(7), 2737–2748. https://doi.org/10.1007/s00382-016-3498-4

Huang, B., Thorne, P. W., Banzon, V. F., Boyer, T., Chepurin, G., Lawrimore, J. H., et al. (2017). Extended reconstructed sea surface temperature, Version 5 (ERSSTv5): Upgrades, validations, and intercomparisons. *Journal of Climate*, *30*(20), 8179–8205. https://doi.org/10.1175/JCLI-D-16-0836.1

Ilyina, T., Li, H., Spring, A., Müller, W. A., Bopp, L., Chikamoto, M. O., et al. (2021). Predictable variations of the carbon sinks and atmospheric CO_2 growth in a multi-model framework. *Geophysical Research Letters*, *48*(6), e2020GL090695. https://doi.org/10.1029/2020gl090695

Izumo, T., Vialard, J., Lengaigne, M., de Boyer Montegut, C., Behera, S. K., Luo, J.-J., et al. (2010). Influence of the state of the Indian Ocean dipole on the following year's El Niño. *Nature Geoscience*, *3*(3), 168–172. https://doi.org/10.1038/ngeo760

Jacox, M. G., Alexander, M. A., Amaya, D., Becker, E., Bograd, S. J., Brodie, S., et al. (2022). Global seasonal forecasts of marine heatwaves. *Nature*, *604*(7906), 486–490. https://doi.org/10.1038/s41586-022-04573-9

Jeon, W., Park, J.-Y., Stock, C. A., Dunne, J. P., Yang, X., & Rosati, A. (2022). Mechanisms driving ESM-based marine ecosystem predictive skill on the east African coast. *Environmental Research Letters*, *17*(8), 084004. https://doi.org/10.1088/1748-9326/ac7d63

Jeong, J. I., Park, R. J., Yeh, S.-W., & Roh, J.-W. (2021). Statistical predictability of wintertime PM2.5 concentrations over East Asia using simple linear regression. *Science of the Total Environment*, *776*, 146059. https://doi.org/10.1016/j.scitotenv.2021.146059

Jiang, F., Zhang, W., Jin, F.-F., Stuecker, M. F., & Allan, R. (2021). El Niño pacing orchestrates inter-basin Pacific–Indian Ocean interannual connections. *Geophysical Research Letters*, *48*(19), e2021GL095242. https://doi.org/10.1029/2021GL095242

Joh, Y., & Di Lorenzo, E. (2019). Interactions between Kuroshio Extension and Central Tropical Pacific lead to preferred decadal-timescale oscillations in Pacific climate. *Scientific Reports*, *9*(1), 13558. https://doi.org/10.1038/s41598-019-49927-y

Kämpf, J., & Chapman, P. (2016). The California current upwelling system. In J. Kämpf & P. Chapman (Eds.), *Upwelling systems of the world: A scientific journey to the most productive Marine ecosystems* (pp. 97–160). Springer International Publishing. https://doi.org/10.1007/978-3-319-42524-5_4

Kang, X., Zhang, R.-H., Gao, C., & Zhu, J. (2017). An improved ENSO simulation by representing chlorophyll-induced climate feedback in the NCAR Community Earth System Model. *Scientific Reports*, *7*(1), 17123. https://doi.org/10.1038/s41598-017-17390-2

Klein, S. A., Soden, B. J., & Lau, N.-C. (1999). Remote sea surface temperature variations during ENSO: Evidence for a tropical atmospheric bridge. *Journal of Climate*, *12*(4), 917–932. https://doi.org/10.1175/1520-0442(1999)012<0917:Rsstvd>2.0.Co;2

Kug, J.-S., Jin, F.-F., & An, S.-I. (2009). Two types of El Niño events: Cold Tongue El Niño and warm pool El Niño. *Journal of Climate*, *22*(6), 1499–1515. https://doi.org/10.1175/2008jcli2624.1

21699291, 2022, 10, Downloaded from https://agupubs.onlinelibrary.wiley.com/doi/10.1029/2022JC019121, Wiley Online Library on [22/10/2022]. See the Terms and Conditions (https://onlinelibrary.wiley.com/terms-and-conditions) on Wiley Online Library for rules of use; OA articles are governed by the applicable Creative Commons License

Kug, J.-S., & Kang, I.-S. (2006). Interactive feedback between ENSO and the Indian Ocean. *Journal of Climate*, *19*(9), 1784–1801. https://doi.org/10.1175/jcli3660.1

Laws, E. A., DiTullio, G. R., & Redalje, D. G. (1987). High phytoplankton growth and production rates in the North Pacific subtropical gyre1, 2. *Limnology & Oceanography*, *32*(4), 905–918. https://doi.org/10.4319/lo.1987.32.4.0905

Lee, K.-W., Yeh, S.-W., Kug, J.-S., & Park, J.-Y. (2014). Ocean chlorophyll response to two types of El Niño events in an ocean-biogeochemical coupled model. *Journal of Geophysical Research: Oceans*, *119*, 933–952. https://doi.org/10.1002/2013JC009050

Lim, H.-G., Dunne, J. P., Stock, C. A., Ginoux, P., John, J. G., & Krasting, J. (2022). Oceanic and atmospheric drivers of post-El-Niño chlorophyll rebound in the equatorial Pacific. *Geophysical Research Letters*, *49*(5), e2021GL096113. https://doi.org/10.1029/2021GL096113

Luo, J.-J., Liu, G., Hendon, H., Alves, O., & Yamagata, T. (2017). Inter-basin sources for two-year predictability of the multi-year La Niña event in 2010–2012. *Scientific Reports*, *7*(1), 2276. https://doi.org/10.1038/s41598-017-01479-9

Manizza, M., Le Quéré, C., Watson, A. J., & Buitenhuis, E. T. (2005). Bio-optical feedbacks among phytoplankton, upper ocean physics and sea-ice in a global model. *Geophysical Research Letters*, *32*(5), L05603. https://doi.org/10.1029/2004GL020778

Mantua, N. J., Hare, S. R., Zhang, Y., Wallace, J. M., & Francis, R. C. (1997). A Pacific interdecadal climate oscillation with impacts on salmon production. *Bulletin of the American Meteorological Society*, *78*(6), 1069–1080. https://doi.org/10.1175/1520-0477(1997)078<1069:apicow>2.0.co;2

Maritorena, S., d'Andon, O. H. F., Mangin, A., & Siegel, D. A. (2010). Merged satellite ocean color data products using a bio-optical model: Characteristics, benefits and issues. *Remote Sensing of Environment*, *114*(8), 1791–1804. https://doi.org/10.1016/j.rse.2010.04.002

Maritorena, S., & Siegel, D. A. (2005). Consistent merging of satellite ocean color data sets using a bio-optical model. *Remote Sensing of Environment*, *94*(4), 429–440. https://doi.org/10.1016/j.rse.2004.08.014

Maritorena, S., Siegel, D. A., & Peterson, A. R. (2002). Optimization of a semianalytical ocean color model for global-scale applications. *Applied Optics*, *41*(15), 2705–2714. https://doi.org/10.1364/AO.41.002705

Martinez, E., Gorgues, T., Lengaigne, M., Fontana, C., Sauzède, R., Menkes, C., et al. (2020). Reconstructing global chlorophyll-a variations using a Non-linear statistical approach. *Frontiers in Marine Science*, *7*. https://doi.org/10.3389/fmars.2020.00464

McPhaden, M. J., Zebiak, S. E., & Glantz, M. H. (2006). ENSO as an integrating concept in Earth science. *Science*, *314*(5806), 1740–1745. https://doi.org/10.1126/science.1132588

Messié, M., & Chavez, F. P. (2012). A global analysis of ENSO synchrony: The oceans' biological response to physical forcing. *Journal of Geophysical Research*, *117*, C09001. https://doi.org/10.1029/2012jc007938

Morel, A. (1988). Optical modeling of the upper ocean in relation to its biogenous matter content(case I waters). *Journal of Geophysical Research*, *93*(10), 749–710. https://doi.org/10.1029/jc093ic09p10749

Murray, J. W., Leinen, M. W., Feely, R. A., Toggweiler, J. R., & Wanninkhof, R. (1992). EqPac: A process study in the central equatorial Pacific. *Oceanography*, *5*(3), 134–142. https://doi.org/10.5670/oceanog.1992.01

Murtugudde, R. G., Signorini, S. R., Christian, J. R., Busalacchi, A. J., McClain, C. R., & Picaut, J. (1999). Ocean color variability of the tropical Indo-Pacific basin observed by SeaWiFS during 1997–1998. *Journal of Geophysical Research*, *104*(C8), 18351–18366. https://doi.org/10.1029/1999JC900135

Noh, K. M., Lim, H.-G., & Kug, J.-S. (2022). Global chlorophyll responses to marine heatwaves in satellite ocean color. *Environmental Research Letters*, *17*(6), 064034. https://doi.org/10.1088/1748-9326/ac70ec

Park, J.-H., Kug, J.-S., Li, T., & Behera, S. K. (2018). Predicting El Niño Beyond 1-year lead: Effect of the Western Hemisphere warm pool. *Scientific Reports*, *8*(1), 14957. https://doi.org/10.1038/s41598-018-33191-7

Park, J.-Y., Dunne, J. P., & Stock, C. A. (2018). Ocean chlorophyll as a precursor of ENSO: An Earth system modeling study. *Geophysical Research Letters*, *45*(4), 1939–1947. https://doi.org/10.1002/2017GL076077

Park, J.-Y., & Kug, J.-S. (2013). Marine biological feedback associated with Indian Ocean Dipole in a coupled ocean/biogeochemical model. *Climate Dynamics*, *42*(1–2), 329–343. https://doi.org/10.1007/s00382-012-1640-5

Park, J.-Y., & Kug, J.-S. (2014). Marine biological feedback associated with Indian Ocean Dipole in a coupled ocean/biogeochemical model. *Climate Dynamics*, *42*(1), 329–343. https://doi.org/10.1007/s00382-012-1640-5

Park, J.-Y., Kug, J.-S., Park, J., Yeh, S.-W., & Jang, C. J. (2011). Variability of chlorophyll associated with El Niño–Southern Oscillation and its possible biological feedback in the equatorial Pacific. *Journal of Geophysical Research*, *116*, C10001. https://doi.org/10.1029/2011jc007056

Park, J.-Y., Kug, J.-S., & Park, Y.-G. (2014). An exploratory modeling study on bio-physical processes associated with ENSO. *Progress in Oceanography*, *124*, 28–41. https://doi.org/10.1016/j.pocean.2014.03.013

Park, J.-Y., Stock, C. A., Dunne, J. P., Yang, X., & Rosati, A. (2019). Seasonal to multiannual marine ecosystem prediction with a global Earth system model. *Science*, *365*(6450), 284–288. https://doi.org/10.1126/science.aav6634

Planton, Y. Y., Guilyardi, E., Wittenberg, A. T., Lee, J., Gleckler, P. J., Bayr, T., et al. (2021). Evaluating climate models with the CLIVAR 2020 ENSO metrics package. *Bulletin of the American Meteorological Society*, *102*(2), E193–E217. https://doi.org/10.1175/BAMS-D-19-0337.1

Polovina, J. J., Howell, E. A., & Abecassis, M. (2008). Ocean's least productive waters are expanding. *Geophysical Research Letters*, *35*(3), L03618. https://doi.org/10.1029/2007GL031745

Polovina, J. J., Howell, E. A., Kobayashi, D. R., & Seki, M. P. (2017). The transition zone chlorophyll front updated: Advances from a decade of research. *Progress in Oceanography*, *150*, 79–85. https://doi.org/10.1016/j.pocean.2015.01.006

Rousseaux, C. S., & Gregg, W. W. (2017). Forecasting ocean chlorophyll in the equatorial Pacific. *Frontiers in Marine Science*, *4*. https://doi.org/10.3389/fmars.2017.00236

Rousseaux, C. S., Gregg, W. W., & Ott, L. (2021). Assessing the skills of a seasonal forecast of chlorophyll in the global pelagic Oceans. *Remote Sensing*, *13*(6), 1051. https://doi.org/10.3390/rs13061051

Saji, N. H., Goswami, B. N., Vinayachandran, P. N., & Yamagata, T. (1999). A dipole mode in the tropical Indian Ocean. *Nature*, *401*(6751), 360–363. https://doi.org/10.1038/43854

Sarmiento, J. L., Slater, R., Barber, R., Bopp, L., Doney, S. C., Hirst, A. C., et al. (2004). Response of ocean ecosystems to climate warming. *Global Biogeochemical Cycles*, *18*(3), GB3003. https://doi.org/10.1029/2003GB002134

Sathyendranath, S., Grant, M., Brewin, R. J. W., Brockmann, C., Brotas, V., Chuprin, A., et al. (2021). *ESA Ocean Colour climate change initiative (Ocean_Colour_cci): Version 5.0 data*. NERC EDS Centre for Environmental Data Analysis. https://doi.org/10.5285/1dbe7a109c0244aaad713e078fd3059a

Séférian, R., Berthet, S., Yool, A., Palmieri, J., Bopp, L., Tagliabue, A., et al. (2020). Tracking improvement in simulated Marine biogeochemistry between CMIP5 and CMIP6. *Current Climate Change Reports*, *6*(3), 95–119. https://doi.org/10.1007/s40641-020-00160-0

Séférian, R., Bopp, L., Gehlen, M., Swingedouw, D., Mignot, J., Guilyardi, E., & Servonnat, J. (2014). Multiyear predictability of tropical marine productivity. *Proceedings of the National Academy of Sciences*, *111*(32), 11646–11651. https://doi.org/10.1073/pnas.1315855111

21699291, 2022, 10, Downloaded from https://agupubs.onlinelibrary.wiley.com/doi/10.1029/2022JC019121, Wiley Online Library on [22/10/2022]. See the Terms and Conditions (https://onlinelibrary.wiley.com/terms-and-conditions) on Wiley Online Library for rules of use; OA articles are governed by the applicable Creative Commons License

Signorini, S. R., Franz, B. A., & McClain, C. R. (2015). Chlorophyll variability in the oligotrophic gyres: Mechanisms, seasonality and trends. *Frontiers in Marine Science*, *2*(1). https://doi.org/10.3389/fmars.2015.00001

Smith, N. R. (1995). An improved system for tropical ocean subsurface temperature Analyses. *Journal of Atmospheric and Oceanic Technology*, *12*(4), 850–870. https://doi.org/10.1175/1520-0426(1995)012<0850:Aisfto>2.0.Co;2

Stuecker, M. F. (2018). Revisiting the Pacific meridional mode. *Scientific Reports*, *8*(1), 3216. https://doi.org/10.1038/s41598-018-21537-0

Taboada, F. G., Barton, A. D., Stock, C. A., Dunne, J., & John, J. G. (2019). Seasonal to interannual predictability of oceanic net primary production inferred from satellite observations. *Progress in Oceanography*, *170*, 28–39. https://doi.org/10.1016/j.pocean.2018.10.010

Talley, L. D., Pickard, G. L., Emery, W. J., & Swift, J. H. (2011). Chapter 14 - global circulation and water properties. In L. D. Talley, G. L. Pickard, W. J. Emery, & J. H. Swift (Eds.), *Descriptive physical Oceanography* (6th ed., pp. 473–511). Academic Press. https://doi.org/10.1016/B978-0-7506-4552-2.10014-9

Tang, W., Llort, J., Weis, J., Perron, M. M. G., Basart, S., Li, Z., et al. (2021). Widespread phytoplankton blooms triggered by 2019–2020 Australian wildfires. *Nature*, *597*(7876), 370–375. https://doi.org/10.1038/s41586-021-03805-8

Tian, F., Rong-Hua, Z., & Xiujun, W. (2021). Indian Ocean warming as a potential trigger for super phytoplankton blooms in the eastern equatorial Pacific from El Niño to La Niña transitions. *Environmental Research Letters*, *16*(5), 054040. https://doi.org/10.1088/1748-9326/abf76f

Tian, F., Zhang, R.-H., & Wang, X. (2020). Effects on ocean biology induced by El Niño-Accompanied positive freshwater flux anomalies in the tropical Pacific. *Journal of Geophysical Research: Oceans*, *125*, e2019JC015790. https://doi.org/10.1029/2019JC015790

Timmermann, A., An, S. I., Kug, J. S., Jin, F. F., Cai, W., Capotondi, A., et al. (2018). El Niño–Southern oscillation complexity. *Nature*, *559*(7715), 535–545. https://doi.org/10.1038/s41586-018-0252-6

Tommasi, D., Stock, C. A., Hobday, A. J., Methot, R., Kaplan, I. C., Eveson, J. P., et al. (2017). Managing living marine resources in a dynamic environment: The role of seasonal to decadal climate forecasts. *Progress in Oceanography*, *152*, 15–49. https://doi.org/10.1016/j.pocean.2016.12.011

Trenberth, K., & Hurrell, J. (1995). Decadal coupled atmosphere. *Climate Change and Northern Fish Populations*, (121), 15.

Trenberth, K. E. (1997). The definition of El Niño. *Bulletin of the American Meteorological Society*, *78*(12), 2771–2778. https://doi.org/10.1175/1520-0477(1997)078<2771:TDOENO>2.0.CO;2

Vallès-Casanova, I., Lee, S.-K., Foltz, G. R., & Pelegrí, J. L. (2020). On the spatiotemporal diversity of Atlantic Niño and associated rainfall variability over west Africa and South America. *Geophysical Research Letters*, *47*(8), e2020GL087108. https://doi.org/10.1029/2020GL087108

Vantrepotte, V., & Mélin, F. (2009). Temporal variability of 10-year global SeaWiFS time-series of phytoplankton chlorophyll a concentration. *ICES Journal of Marine Science*, *66*(7), 1547–1556. https://doi.org/10.1093/icesjms/fsp107

Vimont, D. J. (2005). The contribution of the interannual ENSO cycle to the spatial pattern of decadal ENSO-like variability. *Journal of Climate*, *18*(12), 2080–2092. https://doi.org/10.1175/jcli3365.1

Vimont, D. J., Alexander, M., & Fontaine, A. (2009). Midlatitude excitation of tropical variability in the Pacific: The role of thermodynamic coupling and seasonality. *Journal of Climate*, *22*(3), 518–534. https://doi.org/10.1175/2008jcli2220.1

Vimont, D. J., Wallace, J. M., & Battisti, D. S. (2003). The seasonal footprinting mechanism in the Pacific: Implications for ENSO. *Journal of Climate*, *16*(16), 2668–2675. https://doi.org/10.1175/1520-0442(2003)016<2668:tsfmit>2.0.co;2

Walker, G., & Bliss, E. (1932). Memoirs of the royal meteorological society. *World Weather*, *4*, 53–84.

Xie, S.-P., & Carton, J. A. (2004). Tropical Atlantic variability: Patterns, mechanisms, and impacts. In *Earth's climate* (pp. 121–142). https://doi.org/10.1029/147GM07

Yamaguchi, R., Rodgers, K. B., Timmermann, A., Stein, K., Schlunegger, S., Bianchi, D., et al. (2022). Trophic level decoupling drives future changes in phytoplankton bloom phenology. *Nature Climate Change*, *12*(5), 469–476. https://doi.org/10.1038/s41558-022-01353-1

Yeh, S.-W., Cai, W., Min, S. K., McPhaden, M. J., Dommenget, D., Dewitte, B., et al. (2018). ENSO atmospheric teleconnections and their response to greenhouse gas forcing. *Reviews of Geophysics*, *56*(1), 185–206. https://doi.org/10.1002/2017RG000568

Yeh, S. W., Kug, J. S., Dewitte, B., Kwon, M. H., Kirtman, B. P., & Jin, F. F. (2009). El Nino in a changing climate. *Nature*, *461*(7263), 511–514. https://doi.org/10.1038/nature08316

Yoder, J. A., & Kennelly, M. A. (2003). Seasonal and ENSO variability in global ocean phytoplankton chlorophyll derived from 4 years of SeaWiFS measurements. *Global Biogeochemical Cycles*, *17*(4), 1112. https://doi.org/10.1029/2002GB001942

Zebiak, S. E. (1993). Air–Sea interaction in the equatorial Atlantic region. *Journal of Climate*, *6*(8), 1567–1586. https://doi.org/10.1175/1520-0442(1993)006<1567:Aiitea>2.0.Co;2

Zebiak, S. E., & Cane, M. A. (1987). A model El Ni&ntilde–Southern oscillation. *Monthly Weather Review*, *115*(10), 2262–2278. https://doi.org/10.1175/1520-0493(1987)115<2262:Ameno>2.0.Co;2

Zhang, R.-H., Tian, F., & Wang, X. (2018). Ocean chlorophyll-induced heating feedbacks on ENSO in a coupled ocean physics–biology model forced by prescribed wind anomalies. *Journal of Climate*, *31*(5), 1811–1832. https://doi.org/10.1175/jcli-d-17-0505.1

21699291, 2022, 10, Downloaded from https://agupubs.onlinelibrary.wiley.com/doi/10.1029/2022JC019121, Wiley Online Library on [22/10/2022]. See the Terms and Conditions (https://onlinelibrary.wiley.com/terms-and-conditions) on Wiley Online Library for rules of use; OA articles are governed by the applicable Creative Commons License